DEPARTMENT OF ELECTRICAL ENGINEERING
ELECTROPHYSICS

Mode selection by Priming in an Overmoded Electron Cyclotron Maser*

Alan H. McCurdy

Department of Electrical Engineering, University of Southern California, Los Angeles, CA 90089-0271

Final Report for Contract N00014-89-J-2044

for the period

September 25, 1989 to September 24. 1990

Prepared for the Naval Research Laboratory,

Washington, D.C. 20375-5000

*** The research described in this report was carried out in collaboration with C.M. Armstrong of the Naval Research Laboratory.**

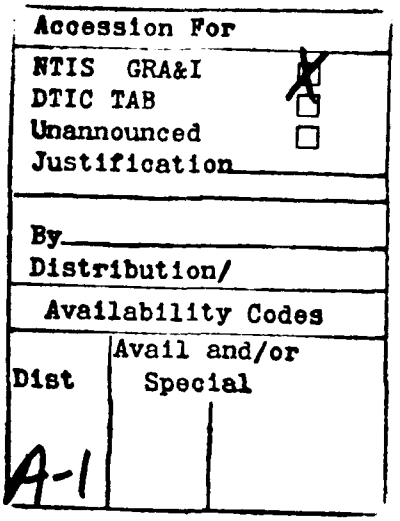

Mode selection by Priming in an Overmoded Electron Cyclotron Maser

ABSTRACT

It is been found that an externally injected signal can strongly influence the steady-state electromagnetic mode in which a pulsed electron cyclotron maser (ECM) operates. A careful experimental examination reveals that the process by which this occurs is similar to the oscillator phase priming noted previously in magnetron work. It is found here that the degree of mode control depends on the injected signal power level (relative to the ECM noise power level), frequency, and time of application. Mode control is obtained at power levels nearly four orders of magnitude below that of the steady-state ECM output power and over frequency bandwidths several times that of the cavity resonance band. The optimum input signal is a circularly polarized wave, co-rotating with the electron cyclotron motion. The experimental results are compared with a quasilinear coupled-mode theory. The theory is used to provide analytic predictions of the temporal mode evolution through third order coupling. The comparison with experiment indicates that higher order terms are non-negligible in some regimes of operation. However, this model suitably predicts ECM steady state operation over much of the operating parameter space and gives a qualitative understanding of the role of the external signal and pre-oscillation noise in the mode selection process. Mode priming may enable stable and efficient single-mode operation of the ECM and other overmoded sources of coherent radiation.

I. INTRODUCTION

It has been previously demonstrated that pure, single-mode operation can be achieved in a overmoded rf oscillator (electron cyclotron maser) via injection of an external signal.[1] The observed phenomenon showed qualitative agreement with a simple theory based on Lamb's quasi-linear treatment[2] of the multimode problem in lasers. Here we present more detailed experimental evidence of this effect and make a *quantitative* comparison with the quasi-linear theory appropriate for the electron cyclotron maser (ECM).[3]

Sources of coherent radiation typically suffer from competition between different spatial electromagnetic modes when the operating frequency becomes high enough that the corresponding free space wavelength is small compared to the characteristic source dimensions. This competition has a variety of deleterious effects but primary among them are losses in source efficiency, spectral degradation of the output radiation, and perhaps undesirable thermal loading or electrical breakdown in the source components. Consequently a variety of techniques have been developed to either prevent the excitation or provide suppression of unwanted electromagnetic modes. Interferometric methods involving a modified cavity structure have been used in lasers and similar slotted or complex cavities have been used to stabilize lower frequency rf oscillators. Another common technique at all frequencies is the introduction of selective loss into the cavity to resistively damp unwanted modes. These techniques, though successful in some limited cases, have the common problem of being rather inflexible, difficult designs which often are only successful over a narrow region of operating parameters. In addition, pure single-mode operation at the optimum efficiency predicted by single-mode theory is rarely, if ever, achieved.

On the other hand, it has been known for some time that the steady state conditions of a nonlinear oscillator can strongly depend on the initial conditions (pre-oscillation conditions). The work on oscillator phase control in magnetrons by David[4] clearly demonstrated this phenomenon in the field of coherent radiation sources. David showed that by applying a small external rf signal during the early stages of oscillation build-up, the final relative phase between the magnetron and external source

could be controlled. The degree to which control was maintained depended on the relative size of the external signal to the magnetron pre-oscillation noise level. The steady state magnetron frequency was unaffected by the external source, and hence no phase locking occurred (evidently the external power level was orders of magnitude below that required for phase locking at any given frequency separation between the magnetron and the external source). This effect was termed *phase priming* in an obvious analogy to the priming of a pump. More recent experiments have verified David's results in the magnetron[5,6] and the ECM.[7]

The identifying features of a *priming* phenomenon, as defined by this early magnetron work, are as follows: (1) the external signal has an observable effect on the steady state oscillation; (2) the external signal only has this effect if it is applied in the early stages of oscillation growth (the oscillator ignores the tiny external signal during the steady state, and hence there is no change in the operating frequency or output power); (3) the effect is one of degree (as opposed to the definite threshold associated with the onset of phase locking); (4) the degree of priming depends on (a) the power level of the external source relative to that of the pre-oscillation noise, (b) the frequency separation between the external signal and oscillator (this dependence is weak and set largely by the quality factor of the cavity).

Experiments involving mode selection by an external signal were performed on CO_2 TEA and Nd:YAG lasers.[8,9] The phrase *injection seeding* was coined to describe the priming of modes. Since, as will be shown here, this seeding phenomenon matches all four characteristics identified in the earlier work, one might more aptly use the term *mode priming*. In addition, it will be shown that the oscillator phase is, in fact, primed coincidentally with the oscillator mode.

The new results presented here are based on experiments carried out at the Naval Research Laboratory on a 5 GHz electron cyclotron maser. The electron cyclotron maser mechanism involves the interaction of a cyclotron wave on an electron beam with a co-propagating transverse electromagnetic wave. The negative mass instability enables efficient emission of radiation. The experimental configuration is given in Fig. 1. The interaction region consists of a cylindrical waveguide near cutoff with a 1.75 cm radius and approximately 10 free space wavelengths in length. Discontinuities

terminate the cavity at the electron gun and collector ends. The electron beam parameters are 20 kV at 2 A with a measured perpendicular-to-parallel velocity ratio, α, of ~ 1.4 (with an accuracy of ~ 20%). Competition is observed between axial TE_{11q} modes at the fundamental and TE_{21q} modes at the second harmonic of the cyclotron frequency. Here q is the axial mode index. Capacitively and inductively coupled probes establish the presence or absence of modes. Because the probes are coupled weakly to the cavity, internal ohmic losses cause the quality factors of the lowest four axial modes all to be ~ 1200. It is clear that there will be significant mode competition if the transit time broadening is larger than the inter-mode frequency spacing. For axial modes in an ECM the criterion is

$$2q - 1 < \frac{4\omega_n L}{\pi c}\beta_z \quad ,$$

where ω_n is the frequency of mode n, L is the cavity length, and β_z is the ratio of the axial electron velocity to the speed of light c. From this relation it can be seen that since the modes become farther apart in frequency as the axial mode index increases, then the mode competition decreases. On the other hand, the mode competition increases with β_z, because of transit time broadening, and increases with ω_n and L because of closer mode spacing. Note that the effect of increased transit time by increase of L (hence decreasing the transit time broadening and therefore the degree of mode competition) is overcome by the effect of L on the mode spacing. In this experiment, the right hand side of the above expression is ~ 15, which is much larger than the spacing between the low order modes.

The general philosophy behind these experiments is as follows. The electron beam is modulated with the priming signal via electron cyclotron resonance absorption. If the beam modulation is at a frequency close to that of the desired mode, then that mode will be given an advantage in the ensuing mode competition which develops as the electron beam excites all modes within the cyclotron resonance band. There is no *a priori* justification, however, for expecting such a simple sequence of events. In particular, the modes may not be strongly coupled or one mode may excite rather than suppress another. It is these concerns which motivate the development of a valid theoretical model.

It is found experimentally that mode control can be obtained in a variety of different situations. When the unperturbed ECM oscillation skips between two or more modes from pulse to pulse, any of the modes can be selected by a priming signal at the appropriate frequency. Also oscillation in a single stable mode can be switched to another nearby mode over a restricted range of operating parameters. Finally, a case is studi d where a bistable system (two simultaneously oscillating modes) is reduced to a single mode because of the priming signal. Other experiments show that optimal mode priming occurs when the input signal is launched as a circularly polarized wave which co-rotates with the electron cyclotron motion. Using the degree of mode control as a measure of coupling between the electromagnetic wave and the electron beam it is found that the ratio of coupling factors for the right- and left-circularly polarized waves is near that predicted from theory.[10]

Using symbolic logic manipulation, analytic results are obtained for the linear growth rate and self- and cross-saturation coefficients for any circular $TE_{m\ell q}$ mode in the ECM. These complex coefficients then are used in the rate equations for the temporal evolution of amplitude and phase of each mode. This description of the mode evolution is displayed in phase plots (as originally done by Lamb[2]) to reveal the basins of attraction of the various stable equilibria. The pre-oscillation noise and the priming signal can be approximately included in this description as initial conditions from which the system evolves. The case considered here is a simple one: two modes interacting solely through their amplitudes. It is found experimentally that such a situation does exist for particular values of the ECM operating parameters. This experiment is compared quantitatively with the quasi-linear theory.

The paper is organized as follows. In Sec. II we review the quasi-linear multimode theory. In this approximation, the rate equations are derived and the coefficients of these equations are determined analytically up to third order. In Sec. III the experimental evidence is presented for mode priming which includes the dependencies on power, frequency, polarization, and time of application of the input signal. Section IV contains an interpretation of the experimental results and includes a quantitative comparison between theory and experiment. The conclusions are given in Sec. V.

II. QUASI-LINEAR THEORY

A. Rate equations for the electromagnetic modes

The development of the quasi-linear theory of mode competition is due to Lamb and has been applied to the ECM by Nusinovich. Here we merely state the assumptions and summarize the procedure for including the external signal and pre-oscillation noise. The goal is to arrive at equations revealing the dynamics of the phase and amplitude of the electric field of the various modes. Starting from a Slater expansion of the cavity fields:[11]

$$\mathbf{E} = \sum_n a_n(t)\,\mathbf{e}_n \quad , \qquad \mathbf{H} = \sum_n b_n(t)\,\mathbf{h}_n \quad ,$$

$$\mathbf{e}_n = \nabla \times \left[f_q(z)\,\Psi_{ml}(\mathbf{r}_\perp)\,\hat{\mathbf{z}} \right] \quad , \quad \mathbf{h}_n = \frac{1}{k_n} \nabla \times \mathbf{e}_n \quad ,$$

$$a_n(t) = \frac{1}{2} A_n(t)\, e^{i\left[\Psi_n(t) + \omega_n t\right]} + \text{c.c.} = \tilde{a}_n(t) + \text{c.c.} \quad ,$$

a wave equation for $\tilde{a}_n(t)$ can be obtained. Here $\mathbf{e}_n$ and $\mathbf{h}_n$ are the orthonormal eigenmodes of the cavity, $f_q(z)$ is the axial profile function (the z axis is directed along the cavity axis, in the direction of the electron beam flow), $\Psi_{m\ell}$ is the transverse cavity eigenfunction, ω_n and k_n are the frequency and wavenumber of the free-running (single-mode) oscillator in the nth mode (n is an abbreviation for the three indices m, ℓ and q). The instantaneous frequency of oscillation is $\omega_n + \dot{\Psi}_n$. The rate equations for the slowly varying amplitude $A_n(t)$ and phase $\Psi_n(t)$ of the electric field of the nth mode can be obtained by separately equating the real and imaginary parts of the wave equation for $\tilde{a}_n(t)$. In doing so, it is assumed that A_n and Ψ_n vary little over a period of the field oscillation $2\pi/\omega_n$. Furthermore, the good cavity assumption $1/Q_o \sim 1/Q_e << 1$ is used where the Ohmic wall loss and external quality factors are given by Q_o and Q_e. If the ac part of the beam current density is also small, then the rate equations can be written

$$\frac{d}{dt}\Psi_n + \frac{1}{2}\left[\omega_n - \frac{1}{A_n}\mathrm{Re}\{L\} - \frac{\omega_n^{o\,2}}{\omega_n}\right] + \frac{\omega_n}{2}\mathrm{Re}\{\chi_n\} = 0 \quad ,$$

$$\frac{d}{dt}A_n + \frac{1}{2}\mathrm{Im}\{L\} + \frac{\omega_n A_n}{2}\mathrm{Im}\{\chi_n\} = 0 \quad . \qquad (1)$$

Here ω_n^o is the cold cavity resonant frequency of the nth mode and L is defined by

$$L = \sum_{n'}\left[\frac{(1+i)\,k_n}{k_{n'}Q_o^{nn'}} + \frac{1}{Q_e^{nn'}}\right] i\, A_{n'}\omega_{n'} e^{i\left[\left(\omega_{n'}-\omega_n\right)t + \Psi_{n'} - \Psi_n\right]} \quad , \qquad (2)$$

where $Q_o^{nn'}$ and $Q_e^{nn'}$ are the cross-coupling quality factors between modes n and n'. The electronic susceptibility χ_n is defined as

$$\chi_n = -i\frac{J_n(t)}{\omega_n \varepsilon_o A_n} \quad , \qquad (3)$$

where $J_n(t)$ is the slowly varying amplitude of the ac electron beam current density:

$$\mathbf{J}(\mathbf{r},t) = \frac{1}{2}\sum_n\left[J_n(t)e^{i\left[\Psi_n(t)+\omega_n t\right]} + \mathrm{c.c.}\right]\mathbf{e}_n(\mathbf{r}) \quad . \qquad (4)$$

It is interesting to note that the external priming signal can be introduced to the oscillation in two ways. If the signal is coupled to the electron beam before it enters the oscillator (pre-modulation) then the current density of Eq. (4) must contain a component which oscillates at the drive frequency.[12] This method of injection has been shown to be preferential for ECM phase locking[13] and phase priming[7] since driver isolation can be maintained, optimal coupling to the electron beam can be achieved, and amplification of the drive occurs. If the signal is coupled directly to the oscillator cavity then a modification must be made to the surface integrals in the wave equation. For the purposes of the current discussion, the external signal is included as an initial condition for the rate equations and is not

consistently incorporated into the equations. This approximation simplifies the resulting analysis and is justified as long as the external signal is so small that the oscillation rapidly grows to such a size that it is unaffected by the external signal. Since $A_n / \dot{A}_n >> 2\pi/\omega_d$ (ω_d is the priming frequency) then it is clear that many cycles of the imposed signal will pass before the oscillation will be able to outgrow the priming signal. For this reason there is a frequency dependence to the priming phenomenon. The theory discussed here is unable to predict this dependence.

The electronic susceptibility of Eq. (3) depends on the Fourier components of the current density and hence on the electron dynamics. Thus, to solve for χ_n, one must solve the electron equations of motion which, in turn, depend on the electromagnetic fields. If the electron transit time through the cavity is very rapid, then the field quantities A_n and Ψ_n remain approximately constant. In this way the electron dynamics are adiabatically eliminated from the problem and the electron current density is written as functions of A_n and Ψ_n. The current density can be expanded in powers of the small quantity

$$\delta = \frac{e\,|E_{orbit}|\,2\pi\,r_L}{\frac{1}{2} m_e v_{\perp_o}^2} \quad ,$$

where e, m_e, r_L, and $v_{\perp o}$ are the electronic charge, mass, Larmor radius, and perpendicular (to the static magnetic field) velocity at the cavity entrance, respectively. The electric field magnitude on the electron orbit is denoted by $|E_{orbit}|$. The requirement $\delta << 1$ implies that the electron loses only a small fraction of its total perpendicular kinetic energy in a period of its cyclotron motion. This requirement is typically satisfied for a resonant interaction (such as the ECM) which requires the electron period to be well defined, thus implying many electron cycles in the interaction region.

The susceptibility can now be written in a power series:

$$\chi_n \equiv \frac{1}{\omega_n A_n} \left\{ \sum_\sigma A_\sigma\, e^{i\left[(\omega_b - \omega_h)\,t + \Psi_\sigma - \Psi_n\right]}\, \alpha_{n\sigma} + \sum_\sigma \sum_\nu \sum_\rho A_\sigma\, A_\nu\, A_\rho\, e^{i\Phi_{\sigma\nu\rho n}}\, \theta_{\sigma\nu\rho n} + \ldots \right\} \quad , \qquad (5)$$

where $$\Phi_{\sigma\nu\rho n} = \left(\omega_\sigma - \omega_\nu + \omega_\rho - \omega_n\right) t + \Psi_\sigma - \Psi_\nu + \Psi_\rho - \Psi_n \quad ,$$

and the summations are over all possible modes. If the frequency separation between modes is much larger than the mode linewidths, then Eqs. (1) and (2) can be averaged over the fast time scale of the intermode phase beating. If, in addition, there are no degenerate modes and the modes are unequally spaced in frequency, then the amplitude equation becomes independent of the mode phases. Expanding the time-averaged electronic susceptibility to third order using the typical notation for the growth rate and saturation coefficients:

$$\bar{\chi}_n = \frac{1}{\omega_n}\left\{ \alpha_n + \beta_n A_n^2 + \sum_\nu \gamma_{n\nu} A_\nu^2 \right\} \quad , \text{ and } \quad L_n = \left[\frac{(i-1)}{Q_o^n} + \frac{i}{Q_e^n}\right] A_n \omega_n \quad , \tag{6}$$

where the replacements $\alpha_{n\sigma} \rightarrow \alpha_n$, $\theta_{nnnn} \rightarrow \beta_n$, $\theta_{nvvn} \rightarrow \gamma_{nv}$ have been made. Using Eqs. (6) in Eqs. (1) there results a sequence of rate equations for the slowly varying amplitudes and phases of the various modes. For the purpose of comparison with experiment, it is convenient to write these equations in terms of the power developed in the cavity rather than the field amplitude:

$$\frac{d}{dt}\Psi_n + \omega_n = \omega_n^o + \frac{1}{2} \mathrm{Re}\left\{\alpha_n - \beta_n P_n - \sum_\nu \gamma_{nv} P_v\right\} \quad , \tag{7a}$$

$$\frac{d}{dt} P_n = \mathrm{Im}\left\{\alpha_n P_n - \beta_n P_n^2 - P_n \sum_\nu \gamma_{nv} P_v\right\} \quad . \tag{7b}$$

The coefficients in Eqs. (7) are related to those in Eq. (5) as follows:

$$\alpha_n = -\left[\frac{(1+i)}{Q_o^n} + \frac{i}{Q_e^n}\right] \omega_n - \alpha_{n\sigma}, \quad \beta_n = \frac{2\,Q_o^n}{\omega_n\,\varepsilon_o}\,\theta_{nnnn} \text{ , and } \quad \gamma_{nv} = \frac{2\,Q_o^v}{\omega_v\,\varepsilon_o}\,\theta_{nvvn} \quad . \tag{8}$$

The Q_o in these formulae originate in the transformation from amplitude to power using the definition: $Q_o = \omega \times$ (stored cavity energy)/(power dissipated in cavity walls).

B. Evaluation of the rate coefficients

The quantities $\alpha_{n\sigma}$, θ_{nnnn}, and θ_{nvvn} are found from the electron equations of motion considering the electromagnetic fields to be fixed. Nusinovich[3] has shown that the electron equations of motion, in the slow-time scale formulation, can be written as an iterative sequence of equations for the perpendicular electron momentum expanded in powers of δ. The momentum obtained may then be used to find $\mathbf{J}(r,t)$ in Eq. (4), which in turn yields $J_n(t)$. Using Eq. (3), χ_n and each of its expansion coefficients may be found. Employing the approximation that $\alpha\, \beta_{\perp o}\, \omega_o\, L/(2\, c) >> 1$, the coefficients for a cylindrical cavity and annular electron beam are

$$\alpha_{n\sigma} = \frac{R_n}{e^2}\, \beta_{\perp_o}^4 p_{\perp_o}^2\, \alpha_{n_{reduce}} \quad ,$$

$$\theta_{nnnn} = -\, R_n\, \frac{\left[C_{m\ell} k_{m\ell} J_{m-1}(k_{m\ell} R_o)\right]^2}{\omega_n^2}\, \beta_{n_{reduce}} \quad , \tag{9}$$

$$\theta_{nvvn} = -\, R_n\, \frac{\left[C_{ML} k_{ML} J_{M-1}(k_{ML} R_o)\right]^2}{\omega_v^2}\, \gamma_{nv_{reduce}} \quad .$$

Here α is the ratio of initial perpendicular to parallel electron velocity, $\beta_{\perp o}$ is the ratio of the perpendicular electron velocity to the speed of light, and ω_o is a normalization frequency. The initial perpendicular momentum is $p_{\perp o}$ and the electron beam guiding center radius is R_o. The eigenfunction for a circularly polarized TE cavity mode has been written $\Psi_{m\ell} = C_{m\ell} J_m(k_{m\ell} r) \times \exp(\mp i\, m\, \theta)$, where the perpendicular wavenumber $k_{m\ell} = x_{m\ell}/r_w$ [r_w is the wall radius, $x_{m\ell}$ is the ℓth zero of $J_m'(x)$] and the

constant $C_{m\ell} = \left(J_m(x_{m\ell})\sqrt{\pi\,(x_{m\ell}^2 - m^2)}\right)^{-1}$]. Mode "n" again corresponds to the cylindrical indices m, ℓ, and q which identify the radial, azimuthal, and axial mode numbers. The indices of mode "ν" are M, L, and Q. The factor R_n is defined

$$R_n = \frac{I_o\, e^3}{\gamma_o}\left(1 - \frac{v_{\perp o}^2}{c^2}\right)\frac{[C_{m\ell}\, k_{m\ell}\, J_{m-1}(k_{m\ell} R_o)]^2}{p_{\perp o}^2\, \varepsilon_o\, m_e\, \beta_{\perp o}^8\, \omega_o\, \omega_n} \quad ,$$

where I_o is the dc electron beam current. The factors labelled with a "reduce" subscript are those calculated analytically using the symbolic logic manipulator REDUCE version 3.2.[14] The form of the constants has been given by Nusinovich[3] and these are reproduced in the appendix. These coefficients depend on the axial electric field profile $f_q(z)$, the detuning factor $\Delta_n = 2\,(\omega_n - \Omega)/(\beta_{\perp o}\,\omega_o)$, and the normalized length $\bar{z} = \alpha\,\beta_{\perp o}\,\omega_o\, z/(2\,c)$. Here the electron cyclotron frequency is denoted by Ω. These factors of Eqs. (A1) are used together with Eqs. (9) in Eqs. (8) to find the net linear growth rate and coefficients of self- and cross- saturation for the rate equations (7). Note that the axial field profile is not computed self-consistently in this approximation. A sinusoidal profile is used to model the high quality factor modes of the experiment:

$$f_q(\bar{z}) = \sqrt{\frac{2}{\bar{L}}}\,\sin\left(\frac{q\,\pi}{\bar{L}}\,\bar{z}\right) \quad .$$

Figure 2(a) shows the imaginary part of α_n, which is proportional to the linear growth rate, for the four lowest order TE_{11q} modes. α_n is plotted against the static axial magnetic field using typical experimental parameters (beam current of 2 A, beam voltage 20 kV, α of 1.4). In all calculations, the beam perpendicular velocity is assumed constant though the static axial magnetic field is varied. Growth occurs when the imaginary part of α_n becomes positive. There are q regions of strong growth for a TE_{11q} mode. Because of the large areas of overlap (where several modes grow linearly) it can be expected that there will be mode competition in this device. The higher order terms

must be included to determine which mode survives in the steady state. A comparison of this quasi-linear theory with experiment is made in Sec. IV.

Figure 2(b) shows the oscillator frequency shifts due to the real part of α_n for the four lowest order modes. This coefficient modifies the frequency of oscillation of each mode via Eq. (7a). It can be seen that the frequency separation between modes is on the order of .5 % of the operating frequency. Though linear theory predicts that the ECM frequency may be either above or below that of the cold cavity resonance, in this experiment it is found that the resonant frequency is always upshifted from that of the cold cavity resonance. It has been found that the higher order terms do reduce the downshifting of the ECM frequency.

C. The oscillator phase space

Since it has been assumed that the modifications to the oscillator frequency due to the electron beam are small ($\dot{\Psi}_n$ is small), then the power rate equations (7b) evolve independently of those for the phases (7a). A convenient way to view the solutions to (7b) is to eliminate the time parameter and plot solutions in the phase space formed by the amplitude (or power) in each mode. This was first done by Lamb.[2] For the simple case of two modes interacting solely through their amplitudes he found three general types of interaction. These he termed strong, weak, and neutral coupling, respectively. Strong coupling implies that only one mode survives to the steady state. This is the condition most often observed in the ECM with a closed cavity configuration. Weak or neutral coupling often involves the simultaneous oscillation of two or more modes. In a short pulse experiment, it is not always clear whether two simultaneous modes are weakly coupled, and will survive indefinitely, or strongly coupled but take a long time to approach the steady state. In such a case one must resort to the mathematical criterion for strong coupling, which is $\gamma_{12}\gamma_{21} > \beta_1\beta_2$. A typical phase diagram for two strongly coupled modes is shown in Fig. 3. The oscillator follows one of the trajectories shown depending on its initial conditions. The origin is an unstable equilibrium so that both modes have positive linear growth. Time increases along each trajectory in the direction of the arrows so that the

oscillator approaches either one of the two pure mode solutions ($P_1 = 0, P_2 = P_2^{sat}$ or $P_1 = P_1^{sat}, P_2 = 0$) in the steady state. There is a separatrix (basin boundary) which separates those trajectories that approach mode 1 in the steady state from those which approach mode 2. This separatrix plays a primary role in the mode evolution. Though its equation cannot be found in an analytic form, it does pass through two known points in the phase plane. One is the origin and the other is the intersection (henceforth referred to as point I) of the two lines $\mathrm{Im}\left\{\alpha_i - \beta_i P_i - \gamma_{ik} P_k\right\} = 0$, denoted by the lines A and B in the figure. As can be seen from Eq. (7b), this point is also an equilibrium point, but it can be shown to be unstable for strongly coupled modes.

A qualitative understanding of the mode priming phenomenon can be obtained by using the phase plane representation of the mode evolution. When the oscillator starts up, it can be assumed that there is a broadband noise radiation field generated predominantly by the electron cyclotron motion. The cavity resonances tend to filter the noise so that there remains significant noise power only near the resonance frequency of each mode. Previous studies indicate that this noise is distributed in amplitude according to a Rayleigh distribution and is randomly phased.[7]

In the case when there is no external signal present, the initial condition from which the oscillator evolves is given by the point with phase plane coordinates $(P_1^{noise}, P_2^{noise})$, where P_i^{noise} is the noise power level in the ith mode. The oscillation will proceed to a pure mode 2 or mode 1 oscillation depending on whether this initial condition is above or below the separatrix. If the mode separation is much less than the cyclotron emission band (this is the usually the case because of doppler broadening) then the noise power in two adjacent modes should be of similar size. Hence the initial condition is usually near the 45^o line in the oscillator phase plane. If the separatrix is also in this vicinity then slight fluctuations in pre-oscillation noise may push the initial condition back and forth across the separatrix from one oscillator pulse to the next. In such a case the oscillator would skip back and forth between modes from pulse to pulse. On the other hand, if the separatrix is far from the 45^o line then nearly pure mode operation would result.

If an external priming signal is applied during the start-up phase of each oscillator pulse, the initial condition from which the oscillation evolves is modified. If the priming signal frequency is close to that of mode 1, for example, then the new P_1 coordinate of the initial condition is the vector sum of the noise power in mode 1 and the priming signal power. Since the P_2 coordinate of the initial condition is unchanged and the priming power is arbitrary, the initial condition can be varied over a wide range of values. In particular, the initial condition can be pushed across the separatrix, thus selecting a new steady state mode with only a small amount of priming power (large compared to the pre-oscillation noise power level).

The equation of the separatrix must be obtained in order to predict the modal evolution. In practice, since the noise and priming power levels are small compared to the steady state saturated power level, the initial conditions of interest are always near the origin. Hence it suffices to know the separatrix in this small region of the phase plane. It can be shown that the equation obeys the power law relation

$$P_2 = C\,(P_1)^{\frac{\alpha_2}{\alpha_1}} \tag{10}$$

near the origin. Here C is an unknown constant which depends on all of the rate equation coefficients. C may be found by numerically integrating Eq. (7b) backward in time from point I which, as previously mentioned, must be on the separatrix. Since the right-hand side of Eqs. (7b) vanishes at point I, the integration must be started from a nearby point which is also on the separatrix. Such a point can be found by linearizing the rate equations (7b) about I. Since I is a saddle point, the equation for the separatrix is a straight line in this vicinity. The starting point for the numerical integration is then chosen to be on this line. A linear regression of the numerical data yields C.

D. Theoretical Missed Pulse Fraction

The degree of control over the oscillator modes is measured by determining the fraction of oscillator pulses *not* in the desired mode (missed pulse fraction, F). This degree of control can be analytically determined if the mean noise power and noise power distribution are known. Given these, the temporal evolution of an arbitrary oscillator pulse is found by randomly selecting a power level from distributions for the power in each competing mode, then comparing the resulting initial condition coordinates to those of the separatrix in the phase plane. After repeating this process for a large number of pulses, the fraction F can be determined.

The following discussion is limited to two competing modes with a priming signal applied to mode 1, the "desired" mode. The probability density P_F of the noise power of an undriven mode (mode 2) follows the modified Rayleigh distribution:

$$P_F(P_2)\,dP_2 = \frac{1}{\bar{N}} e^{-\frac{P_2}{\bar{N}}}\,dP_2 \quad ,$$

where $\bar{N}$ is the mean noise power in the mode ($\bar{N}$ is experimentally determined). The driven mode follows the distribution P_D:

$$P_D(P_1)\,dP_1 = \frac{1}{\bar{N}} e^{-\frac{(P_1+D)}{\bar{N}}} I_0\left(\frac{2\sqrt{P_1 D}}{\bar{N}}\right) dP_1 \quad ,$$

where D is the drive signal power and I_0 is a modified Bessel function.[15] The oscillator will operate in the undesired mode if the initial condition in the phase plane is on the wrong side of the separatrix. For the typical situation shown in Fig. 3, the criterion for a missed pulse is

$$P_1 < S(P_2) \qquad \text{or} \qquad Z = \frac{S(P_2)}{P_1} > 1 \ ,$$

where $P_1 = S(P_2)$ is the equation of the separatrix. To find the probability of a missed pulse one needs the probability of $Z > 1$. It can be shown that the probability density of Z is

$$P_Z(Z)\,dZ = \frac{d}{dz}\left\{ \int_{x=0}^{\infty} P_x(x)\left[1 - e^{-\frac{S^{-1}\left(\frac{Z}{x}\right)}{\bar{N}}}\right]dx \right\} dZ \quad ,$$

where $x = 1/P_1$, P_x is the probability density of x,

$$P_x(x)\,dx = -\frac{1}{\bar{N}\,x^2} e^{-\frac{\left(\frac{1}{x}+D\right)}{\bar{N}}} I_0\left(\frac{2}{\bar{N}}\sqrt{\frac{D}{x}}\right)dx \quad ,$$

and S^{-1} is the inverse of S [i.e. , the equation of the separatrix is $P_2 = S^{-1}(P_1)$]. The missed pulse fraction is the probability of $Z > 1$:

$$F = \int_{Z=1}^{\infty} P_Z(Z)\,dZ = 1 - \int_{x=0}^{\infty} P_x(x)\left[1 - e^{-\frac{S^{-1}\left(\frac{1}{x}\right)}{\bar{N}}}\right]dx \quad . \tag{11}$$

Near the origin, the equation for the separatrix is given by Eq. (10); hence

$$S^{-1}\left(\frac{1}{x}\right) = C\left(\frac{1}{x}\right)^{\alpha_2/\alpha_1} \quad . \tag{12}$$

III. EXPERIMENTAL RESULTS

A. Mode priming the ECM

The priming experiments involve the injection of an external signal through one or more of the coupling probes (Fig. 1) into the ECM cavity. A stable sweep oscillator generates the signal and

attenuators and phase shifter circuits are used to launch waves of different circular polarization. The output from the ECM generally couples to all probes which are terminated in matched loads. The output is monitored on probes L1 and L2 to detect even order axial modes (electric field null at cavity midplane) and probes #3 and #4 to detect odd order modes. The mode of operation is determined from (a) frequency measurements using a tunable bandpass filter in the ECM output line, and (b) measurement of the spatial field profile using the various probes along the cavity axis. More than 40 dB of isolation is used to prevent output power from the ECM from reaching the sweep generator. To further ensure that the priming source is unaffected, a large drive power is used together with directional couplers and attenuators to lower the priming signal to the needed size. In this way the feedback power from the ECM is small compared to the power level at which the priming source operates.

Mode control is experimentally shown to be possible under a variety of circumstances. These include (i) switching from a single steady mode, (ii) selecting between two simultaneously oscillating modes, and (iii) selecting between modes which skip back and forth from pulse to pulse. An example of case iii is given in Fig. 4. The oscilloscope traces show the signal from a crystal detector monitoring the output power of the ECM with beam current of .77 A and magnetic field ~1.87 kG. (This experiment was carried out on a cavity with fewer probes and a different electron gun than previously described.) When no priming signal is applied the ECM skips between the TE_{111} (at 5.093 GHz) and TE_{113} (at 5.141 GHz) modes from pulse to pulse. Throughout a given pulse there is no change in mode. The exposure time of the photograph is ~ 2 seconds which corresponds to over 100 pulses. Thus both modes appear in the picture at the same time. Application of a small priming signal at either the frequency of the TE_{111} or TE_{113} mode allows selection of the respective mode. This is confirmed by frequency measurements using the tunable filter. Figure 4(d) shows the relative phase between the TE_{111} oscillation and that of the priming signal (priming frequency near 5.093 GHz). It can be seen that the ECM initially starts up in phase with the priming signal but soon wanders off because of the slight frequency difference. Thus the ECM is phase primed at the same time that it is mode primed. There is no phase locking since the priming power is so small compared to the ECM output power. This example demonstrates two features

of a priming phenomenon: the external signal has an effect on the steady state oscillation but doesn't change the oscillation frequency or power level.

The temporal dependence of the mode priming phenomenon is shown in Fig. 5. Here the external signal power and ECM output power are simultaneously monitored. In the free-running case (Fig. 5(a)) the ECM skips between the TE_{111} and TE_{113} modes from pulse to pulse. Both modes are apparent in each picture since the digitizing oscilloscope uses interleaved sampling (samples from multiple pulses). The definition of the trace of a given mode is a qualitative measure of the fraction of oscillator pulses in that mode. Hence in the free-running case most of the ECM pulses are in the TE_{113} mode because that trace is brighter. A 50 ns wide priming pulse is applied to the ECM about 350 ns before oscillator saturation in Fig. 5 (b). The priming frequency is that of the TE_{111} mode. The priming signal slightly increases the fraction of pulses in the TE_{111} mode since the lower trace becomes brighter, relative to Fig. 5(a), and the upper trace darkens. Moving the priming pulse about 50 ns later in the oscillation buildup has the dramatic effect shown in Fig. 5(c). Now virtually all ECM pulses are in the TE_{111} mode. Moving the priming pulse another 100 ns closer to the ECM saturation show that its effect weakens (Fig. 5(d)). Thus there is an optimal time at which the external signal should be applied to obtain optimal mode control. If the priming pulse is too early in time, it will decay before the ECM oscillation is initiated. Too late in the buildup and the ECM power is large enough to ignore the priming signal. This temporal dependence of mode control is further evidence that the phenomenon is one of priming. This feature might be exploited when priming a high power oscillator by isolating the priming source from the oscillator during the high power part of the oscillator pulse.

A global picture of mode selection for the TE_{111} mode is shown in Fig. 6. Here the regime of pure TE_{111} mode operation in both the free-running and primed cases are indicated on a plane formed by the operating parameters beam current and axial magnetic field(I-B plane). In the free-running case a complicated pattern of pure modes exists separated by regions of pulse-to-pulse mode skipping. Application of the priming signal allows pure mode operation if the priming frequency is sufficiently close to one of the modes. It can be seen from Fig. 6 that the regime over which a pure TE_{111} mode can be obtained increases by about 40 % when a priming signal is applied. The maximum priming signal power

used was less than 20 W (outside the cavity). The regime of primed TE_{111} operation is found to displace free-running regimes of stable TE_{112}, TE_{114}, TE_{118}, and TE_{119} operation and pulse-to-pulse mode skipping regimes involving these and other modes. Other experiments show that the regime of pure mode operation of each of the higher order axial modes can be enhanced by a priming signal of the appropriate frequency. This priming frequency is very close to the frequency the mode would have, for the given beam current and magnetic field, if it could oscillate alone. In addition, an experiment at the second harmonic of the cyclotron frequency, using TE_{21q} modes at ~ 8.5 GHz, reveals that the same degree of mode control can be obtained.

From these results it is clear that control can be obtained over the steady state mode at the boundary between the excitation of any two modes in the I-B plane. This result is significant since it is a common feature of the ECM that the regime of maximum predicted efficiency is near the boundary of excitation of competing modes. It is to be emphasized that *single-mode operation* does not imply that there is no mode competition. Single-mode operation simply means that the mode coupling only allows a single mode in the steady state. Whether or not that mode can be obtained at optimal efficiency is an issue in which mode competition plays a crucial role. Often single-mode theory predicts a maximal efficiency of a particular mode at a point in the I-B plane where a competing mode is experimentally found. This type of single-mode operation is undesirable. Mode priming may be a means of obtaining the desired mode in such a situation. In addition, it has been noted that the highest efficiency regime for the ECM often occurs for beam currents below the start oscillation current. It has been shown previously that this hard excitation regime is accessible via a priming signal.[12]

Figure 7 shows the minimum drive power required to achieve pure mode operation as a function of priming frequency. Here pure mode operation is defined to mean that greater than 99.95 % of all ECM output pulses are in the desired mode. A magnetic field near 1.84 kG and a 22 kV, .55 A beam yield a steady TE_{113} mode oscillation. The priming signal is at a frequency near that of the TE_{111} mode (5.074 GHz). The experimental points in Fig. 7 generally fall along an inverted Gaussian. There is a slight asymmetry between high priming frequencies ($\Delta\omega > 10$ MHz, where $\Delta\omega \equiv$ difference between priming and TE_{111} frequencies) and low priming frequencies $\Delta\omega < 10$ MHz. The frequency dependence is

not Lorentzian, as would be expected from the cavity resonance profile. It is clear that the change in mode control with drive frequency is not simply due to the finite resonance width of the cavity. The priming power required for a given level of mode control is found to increase exponentially with $\Delta\omega$. Another unusual feature of Fig. 7 is that the frequency at which the least priming power is required for pure mode operation is not the same as the TE_{111} frequency. In this experiment and in all other cases studied (including experiments at the second cyclotron harmonic), better mode control is obtained with a priming signal of frequency slightly above that of the free-running oscillation. This same feature is present whether the competing mode frequency is above or below that of the primed mode. The explanation may be that the oscillation frequency during the build-up is not the same as that during the steady-state (which is the measured frequency). However, the theoretical model presented here allows for no oscillator dynamics due to the priming signal so this unusual feature must be explained using a more detailed description of the build-up scenario. From Fig. 7 it is seen that, when priming at the optimal frequency, the necessary priming power (measured outside the cavity) for pure mode oscillation is nearly three orders of magnitude below the output oscillator power in the TE_{111} mode. When the probe coupling is taken into account, the priming power is nearly four orders of magnitude below the oscillator power inside of the cavity. The bandwidth over which mode control can be maintained is several times the cavity resonance width.

Using a linearly uptapered axial magnetic field it is possible to excite two simultaneously oscillating modes. This is because the cyclotron resonance condition varies along the length of the device. A low frequency mode oscillates near the electron gun (upstream) while a high frequency mode grows in the downstream region. The faster growing mode is downstream of the slower growing one. In this way the downstream mode grows to a large size before encountering any adverse electron beam modulation due to the upstream mode. These modes are still strongly coupled but, since they interact with different parts of the electron beam, the time taken to reach equilibrium is much longer than the pulse length. It is possible to eliminate the faster growing mode entirely by priming the upstream mode. Priming the downstream mode has no effect on the mode evolution. Reversing the direction of

the magnetic field taper causes the faster growing mode to be the upstream mode and thereby eliminates the slower growing mode entirely.

B. Coupling of the priming signal to the electron beam

The degree of mode control obtained by priming is expected to be related to, among other things, the degree of coupling of the input electromagnetic wave to the electron beam. Thus the degree of mode control can be used as an indirect measure of the nature of the electromagnetic wave which participates in the electron cyclotron maser mechanism. Here we show that optimal mode control, for our cavity, occurs when the input wave is launched with circular polarization, co-rotating with the electron cyclotron motion.

The theoretical expression for the perturbation in electron motion by a TE wave contains terms proportional to $(\mp \omega - k_z v_z - n \Omega)^{-2}$. Here k_z is the axial wavenumber, v_z the axial electron velocity and n the cyclotron harmonic number. The largest deviations in electron position are produced by these terms when $\mp \omega - k_z v_z - n \Omega \cong 0$. *Obviously the plus sign in front of ω must be chosen for this* synchronism condition to be satisfied. This means that the electromagnetic wave rotates in the same direction as the beam cyclotron wave. The electrons thus feel virtually static fields in the co-rotating frame of reference. The experimental objective here is to show that regardless of how the electromagnetic wave is polarized, upon injection into the ECM, it is the co-rotating component of the wave which predominantly couples to the electron beam. Because the axial magnetic field is directed opposite to the electron flow, the best coupling is expected to occur via a left-hand circularly polarized electromagnetic wave.

Injecting a signal (at the cyclotron fundamental frequency) into the ECM through a single capacitively coupled probe excites a standing TE_{11} wave. The structure of this field in the cylindrical cavity is given by

$$E = E\left(\frac{1}{k_\perp r} J_1(k_\perp r) \sin\phi\, \hat{r} + \frac{dJ_1(k_\perp r)}{dk_\perp r} \cos\phi\, \hat{\phi}\right) e^{j\omega t} \quad . \tag{13}$$

Here the dependence on axial coordinate is suppressed for compactness of presentation. The polar coordinates are r and ϕ and the probe is located at $\phi = 90^o$ (see Fig. 8(a)). Using the abbreviations

$$A = \frac{1}{k_\perp r} J_1(k_\perp r) \quad \text{and} \quad B = \frac{dJ_1(k_\perp r)}{dk_\perp r} \quad ,$$

the linearly polarized wave in (13) can be written in terms of circularly polarized waves: [16]

$$E = A\left(\frac{E}{2} e^{j(\omega t+\phi+\pi/2)} + \frac{E}{2} e^{j(\omega t-\phi+\pi/2)}\right)\hat{r} + B\left(\frac{E}{2} e^{j(\omega t+\phi)} + \frac{E}{2} e^{j(\omega t-\phi)}\right)\hat{\phi} \quad . \tag{14}$$

Here the right-hand (left-hand) component has a negative (positive) sign in the exponential. The time averaged power in the left-hand circularly polarized (LHCP) component of the wave travelling along with the electron beam is (using the orthogonality of the right- and left- hand circularly polarized waves)

$$\langle P_{LH} \rangle = \frac{E^2}{8} \frac{k_z}{\omega \mu_o} \int_S (A^2 + B^2) r \, d\phi \, dr = \frac{P_{IN}}{2} \quad , \tag{15}$$

where the integration is over the cavity cross-section. It can easily be shown that the power into the right-hand (RHCP) component is identical to that of Eq. (15). Thus half of the probe input power, P_{IN}, goes to the left-hand wave as is expected since the total wave is linearly polarized.

The configuration of the two probe excitation is shown in Fig. 8(b). The probes are spatially separated by 90^o in azimuthal coordinate and are excited with amplitudes E_1 and E_2 and with a phase difference θ. The total drive power into the ECM is $P_1 + P_2 = P_{IN}$. The total field in the input wave is the sum of Eq. (13) (with $E = E_1 e^{j\theta}$), and

$$E_2 = E_2 \left(A \cos\phi \, \hat{r} - B \sin\phi \, \hat{\phi}\right) e^{j\omega t} \quad , \tag{16}$$

the field excited by the second probe. Writing Eq. (16) in terms of circularly polarized waves, adding it to Eq. (14), and finding the time averaged power into the right- and left-hand waves as before

$$\langle P \rangle = \frac{1}{2} \frac{k_z}{\omega \mu_o} [E_1^2 + E_2^2 \pm 2 E_1 E_2 \sin\Theta] \int_S (A^2 + B^2) r \, d\phi \, dr \quad , \tag{17}$$

where the upper (lower) sign is taken for the power into the left- (right-) hand circularly polarized wave. For the special case of E_1 leading E_2 by 90^o ($\theta = 90^o$) the power into the left hand wave in Eq. (17) is

$$\langle P_{LH} \rangle = \frac{1}{2} P_{IN} + \sqrt{P_1 P_2} \quad . \tag{18}$$

Further specializing to equal amplitudes injected into the two probes: $\langle P_{LH} \rangle = P_{IN}$, and all of the input power couples to the LHCP electromagnetic wave. As long as the probe diameter is a small fraction of the cavity circumference a pure circularly or linearly polarized wave may be excited. In the experiment, cold test results indicate that the assumption that a single probe excites a pure linearly polarized wave is justified. More than 80 % of the input power was injected into the linearly polarized component.

The degree of control of the modes in the ECM is measured by monitoring the signal from a crystal diode monitoring ECM output power. The ECM is tuned to a parameter region where a single stable mode oscillates in the free-running case. The input priming signal frequency is equal to that of a competing mode. As the drive power couples to the electron beam the ECM begins to mode skip into the driven mode. The input power level is adjusted so that even when the drive power couples optimally to the beam the ECM continues to mode skip to some degree. Two methods of data collection are used. First a simple averaging scheme is used which discriminates the fraction of missed pulses (those not in the primed mode) on the basis of a large difference in amplitude between the primed and free-running

modes. The other method involves actually acquiring a large number of pulses (~ 1000) on a digital oscilloscope and counting the missed pulses using a computer.

The averaging method uses N ECM pulses (N ≅ 256). A certain fraction of these pulses, ρ, will have a level I_1 corresponding to the free-running mode. The remaining fraction of the pulses, (1- ρ), will have the level I_2 of the driven mode. A digitizing oscilloscope provides the average A:

$$A = \frac{1}{N}\left\{\sum_{i=1}^{\rho N}(I_1 + \Delta I_{1_i}) + \sum_{i=1}^{(1-\rho)N}(I_2 + \Delta I_{2_i})\right\} \quad , \tag{19}$$

where random pulse-to-pulse fluctuations in oscillation amplitude, ΔI_i, are included. Equation (19) can be rewritten

$$A = \sum_{i=1}^{\rho N}\frac{\Delta I_{1_i}}{N} + \sum_{i=1}^{(1-\rho)N}\frac{\Delta I_{2_i}}{N} + \rho I_1 + (1-\rho)I_2 \quad . \tag{20}$$

The first two terms in Eq. (20) are assumed to vanish. Though the fluctuations ΔI_1 and ΔI_2 are random from pulse to pulse, their average cannot be neglected unless $\frac{\Delta I}{I} << 1$ and a large number of pulses are included in the average. Though the first condition holds in the experiment the second does not hold in the limits where there is very little control over the free mode or the mode is almost completely controlled. The experimental errors are expected to be correspondingly larger in these regions. The fraction of missed pulses (those not in the driven mode) is therefore $\rho = (A - I_2) / (I_1 - I_2)$. It is this fraction ρ which is the measure of the degree of coupling of the drive signal to the electron beam.

Figure 9 shows the results for priming power injection using one and two probes. The three experiments shown involve measurement of missed pulses (using the averaging method) as a function of priming power. Priming power is injected three different ways and the results are shown as a function of

the power into the LHCP wave in each case. The first experiment is single probe drive. The power into the LHCP wave is determined from Eq. (15). The second experiment consists of driving two probes with equal amplitudes and 90^{o} out of phase. This configuration generates a pure LHCP wave. The last experiment shown in the figure utilizes two probes with arbitrary input amplitudes and 90^{o} out of phase. The power into one probe is held constant while that into the second is varied. Equation (18) is used in this case to determine the coupling to the LHCP wave.

The general result in all the experiments is that, as before, the degree of mode control decreases with decreasing drive power. It is clear from Fig. 9 that regardless of how the amplitude of the drive signal is varied, the degree of mode control depends predominantly upon the drive power in the LHCP wave. From this, it can be inferred that the electromagnetic wave primarily couples to the gyrating electron beam, through electron cyclotron absorption, when the wave is co-rotating with the electrons.

A further test of this conjecture is provided by an experiment in which the drive power is constant but the phase between the two driven probes is varied. The drive power input to each probe is approximately equal. The results of this investigation are shown in Fig. 10. The fraction of missed pulses, ρ, varies approximately sinusiodally with the phase angle θ. This is to be expected if the degree of mode control is simply proportional to the drive power input in a LHCP wave since the power into the two circularly polarized waves in this experiment is [from Eq. (17)]

$$\langle P \rangle = \frac{1}{2} P_{IN} \pm \sqrt{P_1 P_2} \sin \theta \quad . \tag{21}$$

(Figure 9 shows, however, that the relationship between mode control and LHCP drive power is not quite linear.) Of more importance is the location of the points of maximum and minimum mode control. The first minimum of Fig. 10 occurs at ~ 130^{o} (probe #3 leading probe #4 in Fig. 1). When the 32^{o} line length correction is taken into account the point of maximum mode control is found to be ~ 98^{o}. This is quite close to the 90^{o} interprobe phase shift required to produce a pure LHCP wave. The first maximum

occurs at a corrected phase shift of 302°, reasonably close to the 270° required for excitation of a pure RHCP wave.

In conclusion, given a fixed amount of drive power the most efficient means of coupling to the electron beam is at an interprobe phase shift such that a pure LHCP wave is launched into the cavity. Alternatively, given a fixed phase shift between probes the amplitudes should be adjusted so that as much drive power as possible is in the form of a LHCP wave. If the electron beam flow is in the direction of the magnetic field (as is usually the case) then optimal coupling should be obtained with the RHCP wave.

Theory does not predict exactly zero coupling between the RHCP wave and the electron beam or perfect coupling for the LHCP wave when the TE_{11} field pattern and the annular electron beam geometry are taken into account. A more realistic prediction can be made by calculation of the beam-wave coupling coefficient as defined by Chu.[10] The interaction between the beam and the electromagnetic wave is really only dependent on the electric field strength tangential to the electron orbit. The beam power gain is proportional to the square of this electric field. Expanding the electric field of a circular TE_{mn} mode about an off-axis electron gyro-center yields[17]

$$E_\phi = \frac{1}{2} k_{m\ell} C_{m\ell} J_{m-1}(k_{m\ell} R_o) \left[J_0(k_{m\ell} r_L) - J_2(k_{m\ell} r_L) \right] \cos(\omega t - \phi) \quad ,$$

where r_L is the electron Larmor radius. Here only the first spatial harmonic is considered. A thin ring of electrons with guiding centers at a radius R_o is assumed. In the experiment the left-hand wave has eigenvalues m=1, n=1 and the coupling coefficient is

$$K_{LH} = \left\{ J_0(k_{11} R_o) \left[J_0(k_{11} r_L) - J_2(k_{11} r_L) \right] \right\}^2 . \tag{22}$$

The coefficient of the right-hand wave (m=-1, n=1) is

$$K_{RH} = \left\{ J_{-2}(k_{-11} R_o) \left[J_{-2}(k_{-11} r_L) - J_0(k_{-11} r_L) \right] \right\}^2 . \tag{23}$$

Using R_O = .9 cm and r_L = .23 cm (consistent with the beam α), the ratio of the coupling coefficients of Eqs. (22) and (23) equals 55.2. As expected, the theoretical coupling of the co-rotating (LHCP) wave to the beam is much stronger than the oppositely rotating wave. A rough experimental determination of this ratio can be made from the data of Figs. 9 and 10. The missed pulse fraction can be eliminated by transforming ρ in Fig. 10 to power coupled into the left-hand wave using Fig. 9. The curve corresponding to pure left-hand wave excitation in Fig. 9 is used. This power is proportional to the actual power coupled to fields on the electron orbit (Eq. (19) gives the predicted coupling constant). Figure 11 shows the new plot relating phase between the probes to power actually coupled into the fields on the electron orbit. The same sinusoidal shape as Fig. 10 is apparent here.

The power on orbit is produced from the separate contributions of the left- and right-hand circularly polarized waves (as given by Eq. (18):

$$P_{orbit} \sim (P_{IN} + \sqrt{P_1 P_2} \sin\theta)\, K_L + (P_{IN} - \sqrt{P_1 P_2} \sin\theta)\, K_R \quad , \tag{24}$$

where K_R and K_L are proportional to the coupling coefficients of the right- and left-hand polarized waves to the wave on the electron orbit. Varying the coefficients K_R and K_L to match the data in Fig. 11 results in the solid line for a coupling coefficient ratio K_R / K_L of 55.2. The curve has been adjusted for the 10^O systematic error apparent in Fig. 10. There is some difference in the predicted extrema in the sinusoid but the overlap with the experimental points is fairly good. One major uncertainty in this analysis is that the averaging method, upon which the measurement of the missed pulse fraction is based, suffers its largest uncertainty in the regions of very weak and very strong mode control. This means that the data points at the extrema in Fig. 11 are not very accurate. In addition, translating small or large missed pulse fractions into equivalent power via Fig. 9 is not precise. For example, an uncertainty in the missed pulse fraction of 1 % at the maximum point in Fig. 10 causes uncertainties in the coupling ratio of a factor of two since Fig. 9 gives normalized powers anywhere between .5 and 1.5. It is found that variation of the coupling coefficient ratio by a factor of two in

Eq. (18) still produces reasonable agreement with the experimental points in Fig. 11. Thus it can be said only that the measurement of the relative coupling strength of the right- and left-hand waves is in rough agreement with theory.

IV. DISCUSSION

A. Mode coupling

The rate equation coefficients $\alpha_{n_{reduce}}$, $\beta_{n_{reduce}}$, and $\gamma_{nv_{reduce}}$ are functions of three parameters: cavity length L, axial wavenumber k_z, and detuning between the field frequency and cyclotron frequency Δ. If the axial field profile is assumed to be that of the unperturbed cavity mode $f_q(z)$, then $k_z = q\pi/L$ and the parameters are L, q, and Δ. Here we apply these theoretical results to the mode priming experiment.

Figure 12 shows the TE_{111} coefficients as a function of Δ for the experimental situation. The subscript on the coefficients α, β, and γ indicates the q index of the axial mode (hence TE_{111} indicated by 1, TE_{112} by 2, etc.). The quality factors of all modes are 1200, the electron beam voltage is 19.98 kV, beam current is .34 A, perpendicular-to-parallel velocity ratio is 1.4, beam guiding center radius is .9 cm, and the cavity length is 60 cm. The cold cavity resonant frequencies of the lowest order axial modes are 5.033, 5.052, and 5.081 GHz, respectively. The normalization frequency is 5.0 GHz. The detuning parameter Δ_1 in Fig. 12 is calculated using the cold cavity resonant frequency of the TE_{111} mode instead of the exact field frequency. The exact frequency is a function of the real parts of the coefficients as well as the steady state power levels [Eq. (7a)]. This approximation is quite good and can easily be improved by iteration. Figure 12 (a) shows the exact result for α_1, including both the "linear" and "quadratic" bunching terms.[3] Because of this, the growth rate does not equal zero when $\Delta_1 = 0$. For all coefficients, it can be seen that the real and imaginary parts are 90^o "out of phase"; hence the real parts go to zero near the points where the imaginary parts are at an extremum. This implies that, to this degree of approximation, the effect of the electron beam on the field frequency is minimized when Δ_1 is such that maximum growth or saturation occurs. The curves in Fig. 12 are

"universal" in the sense that the oscillator coefficients are related to Δ in the way shown even though the field frequency and power might vary during an iterative calculation. Figure 12 (b) shows β_1 calculated using only the quadratic bunching terms. From Eq. (A1) it can be shown that the imaginary part of β must be an even function of Δ while the real part is odd in Δ. In both Figs. 12 (b) and (c) it can be seen that the TE_{111} mode can be either suppressed ($Im\{\beta_1\} > 0$ or $Im\{\gamma_{12}\} > 0$) or excited ($Im\{\beta_1\} < 0$ or $Im\{\gamma_{12}\} < 0$) by the nonlinear effects. Near resonance ($\Delta \equiv 0$) the suppression dominates while for substantial detuning, $\Delta > .5$, there is growth ($Im\{\alpha_1\} > 0$) and the nonlinear terms provide further excitation.

Figure 13 shows the coefficients calculated for the TE_{112} mode as a function of the detuning parameter Δ_2 (found in terms of the cold cavity TE_{112} resonant frequency). There is the same "phase" relationship between the real and imaginary parts of the coefficients as seen in Fig. 12. The main difference is that in Fig. 13 there are *two* regimes of TE_{112} positive linear growth with corresponding suppression by $Im\{\beta_2\}$ and $Im\{\gamma_{21}\}$ on the edges of the excitation region closest to $\Delta_2 = 0$ and excitation on the opposite ends of the growth regimes. Similar results are obtained for higher order axial modes.

For the purposes of comparison with experiment, the imaginary parts of the coefficients are shown as functions of the magnetic field in Fig. 14 for the lowest three modes. The region of positive linear growth, $Im\{\alpha_1\} > 0$, moves to lower magnetic field for higher order modes. This agrees qualitatively with the experimental observations in Fig. 6. The width of the predicted excitation regions are somewhat different than that experimentally observed. This is in large part due to the fact that the coefficients are calculated using the cold cavity resonant frequencies rather than the actual oscillation frequencies. All modes are strongly excited ($Im\{\beta\} < 0$ and $Im\{\gamma\} < 0$) at the low magnetic field edge of the first growth region (1.81 - 1.83 kG). Near the beam-wave resonance point (~1.86 kG for TE_{111}, ~1.85 kG for TE_{112}, ~1.84 kG for TE_{113}) the nonlinear terms become positive and suppress the oscillation. At higher magnetic fields appear regions of $Im\{\alpha\} < 0$ (no linear growth) yet $Im\{\beta\}$ and $Im\{\gamma\} > 0$ (excitation). These are the *hard excitation* regions where the oscillator is not linearly unstable but may oscillate if an external "kick" is supplied. Figure 14 shows that all modes have regions where hard excitation may be provided via TE_{111} ($Im\{\beta_1\} < 0$ in 14 (a) in the interval 1.87 - 1.89

kG, $Im\{\gamma_{21}\} < 0$ in 14 (b) in the interval 1.855 - 1.875 kG, $Im\{\gamma_{31}\} < 0$ in 14 (c) in the interval 1.845 - 1.89 kG) or either of the other two modes in the appropriate regions. This indicates that mode priming could also be effective in the hard excitation regions. There is a loss of frequency selectivity because of the cross-excitation provided by the $\gamma_{n\nu}$. The branches of TE_{112} and TE_{113} growth at high magnetic field are generally strongly damped. Figures 14 (b) and (c) show that $Im\{\gamma\} > 0$ and $Im\{\beta\} > 0$ for the bulk of those regions of $Im\{\alpha\} > 0$ at magnetic fields above 1.86 kG. This is consistent with the experimental observation that at low beam currents the higher order modes appear primarily on the low magnetic field side of the TE_{111} excitation region (see Fig. 6).

B. Fifth order quasi-linear theory

The mode priming experiment was performed at a magnetic field of ~ 1.838 kG. For this magnetic field many axial modes have positive linear growth rates. Table I shows the coefficients corresponding to the experimental parameters. The high order TE_{113} and TE_{114} have larger self- and cross-saturation coefficients than the low order modes. It is found experimentally that no modes other than the TE_{111} and TE_{112} can be detected during the mode evolution. Injection of an external signal at the expected frequency of a weak mode is found to generally enhance the mode amplitude. In this way even very weak modes can be detected. No evidence of such modes was found in this experiment. Thus it can be inferred that the high order modes are strongly damped and do not play a role in the resulting mode evolution.

Table I shows that all third order coefficients for the TE_{111} mode are *negative*. This implies that all modes *excite* the TE_{111}. Since there is no saturation of the TE_{111} to third order, it is clear that fifth order terms must be included. The terms which must be added to Eq. (7 b) are

$$-\mathrm{Im}\left\{P_n \sum_{\nu} \sum_{\mu} \delta_{n\nu\mu} P_\nu P_\mu\right\} \quad .$$

For the case of two competing modes this correction adds three new terms to each rate equation. The new terms in the TE_{111} power rate equation are

$$- \mathrm{Im}\left\{\delta_{111}\right\} P_1^3 - \mathrm{Im}\left\{\delta_{112}\right\} P_1^2 P_2 - \mathrm{Im}\left\{\delta_{122}\right\} P_1 P_2^2 \quad .$$

Since the rate equations now involve second degree polynomials in P_1 and P_2, the critical points lie along second degree curves (see curves A and B in Fig. 15) instead of the straight lines A and B shown in Fig. 3. The curves still play the same role (trajectories have infinite or zero slope when they intersect one of the curves) and their intersection is on the separatrix.

The stability criteria for the single mode oscillation equilibria $(P_1 = 0, P_2 = P_2^{sat})$ and $(P_1 = P_1^{sat}, P_2 = 0)$ shown in Fig. 15 are

$$\alpha_2 > - \mathrm{Im}\{\delta_{222}\} \left(P_2^{sat}\right)^2 \quad , \quad \alpha_1 - \mathrm{Im}\{\gamma_{12}\} P_2^{sat} - \mathrm{Im}\{\delta_{122}\} \left(P_2^{sat}\right)^2 < 0 \qquad \text{and}$$

$$\alpha_1 > - \mathrm{Im}\{\delta_{111}\} \left(P_1^{sat}\right)^2 \quad , \quad \alpha_2 - \mathrm{Im}\{\gamma_{21}\} P_1^{sat} - \mathrm{Im}\{\delta_{211}\} \left(P_1^{sat}\right)^2 < 0 \quad , \qquad (25)$$

respectively. The corresponding criterion for the instability of the intersection point is

$$A_{11} + A_{22} > 0 \qquad \text{and} \qquad A_{21}\, A_{12} > A_{11}\, A_{22} \quad , \qquad (26)$$

where

$$A_{nn} = \alpha_n - 2\,\mathrm{Im}\{\beta_n\} \left(P_n^{sat}\right)^2 - \mathrm{Im}\{\gamma_{nm}\} P_m^{sat} - 3\,\mathrm{Im}\{\delta_{nnn}\} \left(P_n^{sat}\right)^2 - 2\,\mathrm{Im}\{\delta_{nnm}\} P_n^{sat} P_m^{sat}$$

$$- \mathrm{Im}\{\delta_{nmm}\} \left(P_m^{sat}\right)^2 \quad , \qquad n \neq m \, ,$$

$$A_{nm} = - \mathrm{Im}\{\gamma_{nm}\} P_n^{sat} - \mathrm{Im}\{\delta_{nnm}\} \left(P_n^{sat}\right)^2 - 2\,\mathrm{Im}\{\delta_{nmm}\} P_n^{sat} P_m^{sat} \quad , \qquad n \neq m .$$

When the single mode equilibria are stable and the intersection equilibria is unstable, then the modes are strongly coupled (assuming the linear growth rate of both modes is positive). Thus the criteria in Eqs. (25) and (26) are those for strongly coupled modes in the fifth order theory.

The fifth order coefficients are not calculated here but are estimated from the experimental results. The self-saturation $\mathrm{Im}\{\delta_{nnn}\}$ is found from the experimental single-mode steady state power P_n^{sat}:

$$\mathrm{Im}\left\{\delta_{nnn}\right\} = \frac{\mathrm{Im}\left\{\alpha_n\right\} - \mathrm{Im}\left\{\beta_n\right\} P_n^{sat}}{\left(P_n^{sat}\right)^2} .$$

The experimental results give $\mathrm{Im}\{\delta_{111}\} = 4.85 \times 10^5\ \mathrm{J}^{-2}$ and $\mathrm{Im}\{\delta_{222}\} = 3.84 \times 10^5\ \mathrm{J}^{-2}$. The two cross-coupling terms δ_{nnm} and δ_{nmm} perform similar roles and, since neither is known, δ_{nnm} is arbitrarily set to zero. The δ_{nmm} are chosen subject to the constraints of Eqs. (25) and (26) and are fit to the mode priming experiment (data of Fig. 16). The values $\mathrm{Im}\{\delta_{122}\} = 1.613 \times 10^6\ \mathrm{J}^{-2}$ and $\mathrm{Im}\{\delta_{211}\} = 3.0 \times 10^5\ \mathrm{J}^{-2}$ are obtained in this way. The modal evolution using the set of coefficients through fifth order is shown in Fig. 15. The curves A and B are ellipses in this case. The equation of the separatrix is found in the way previously described.

C. Comparison of mode priming theory and experiment

Figure 16 shows the experimental results of priming a TE_{111} mode from a pure TE_{112} mode. The drive signal polarization is adjusted for optimal mode control. As the drive signal becomes large compared to the mean noise power level (.3 μW) the ECM approaches a pure TE_{111} mode. The solid line shows the results obtained from the theory described in Sec. II D using the coefficients found in Sec. IV B. The theory predicts the missed pulse fraction F that would be observed in a trial experiment consisting of an infinite number of pulses. Since the actual experimental trial length is only 256 pulses, a statistical uncertainty enters when comparing the experiment to the theory. However the standard deviation in missed pulse fraction of a large number of trials of 256 pulses each can be found from the binomial distribution:

$$\sigma_F = \sqrt{\frac{F(1-F)}{256}} \quad .$$

This standard deviation is indicated in Fig. 16 by the error bars. The uncertainty σ_F is small for low drive power because there is a large missed pulse sampling in each trial. At high drive power the uncertainty is a large fraction of F, but is relatively small (compared to intermediate drive levels) since there are few missed pulses detected (F is small).

After taking the statistical uncertainties into account, the theory agrees well with the experimentally measured missed pulse fraction. This indicates that the qualitative explanation for the mode priming phenomenon set forth here has validity. Further, this theory is adequate for prediction of the mode priming power required for a given degree of oscillator control in regions of parameter space where the third order coefficients are positive. A further improvement can be obtained by taking fifth order coefficients into account. This will expand the region of oscillator parameter space over which the theory has applicability. This work is in progress.

V. Conclusion

Injection priming by an external signal is shown to be a powerful and flexible means of mode control in an overmoded electron cyclotron maser. The priming technique makes a much larger region of ECM parameter space accessible to pure mode operation. The technique is effective, to some degree, for all strongly coupled axial modes which otherwise would suffer mode skipping or stable parasitic oscillation. It is anticipated that this technique will also enable control of transverse modes as long as the filling factors of the different modes are similar.

A comparison is made between the experimental mode priming results and a quasi-linear theory of mode competition. It is found that the theory gives a good qualitative picture of the mechanism by which the injected signal selects modes in the strongly coupled case. It is found that for a broadly

applicable quantitative prediction of mode control, terms higher than third order must be included in the theory.

An indirect measurement is made of the relative coupling of the right- and left-hand circularly polarized waves to the electron beam. It is found, as predicted from theory, that the wave with co-rotating polarization is the dominant electromagnetic wave involved in the electron cyclotron resonance mechanism. The experimental relative coupling strength agrees with the theoretical value to within experimental uncertainties.

Acknowledgments

The authors thank B. MacIntosh, S. Swiadek and F. Wood for construction of the electron cyclotron maser tube. The help of W.M. Bollen in experimental setup and R.K. Parker in technical support is gratefully acknowledged. Thanks also to K. Kreischer for suggesting the use of symbolic logic manipulation.

This research was supported by the Office of Naval Research Grant and the Office of Naval Technology. Computer support was provided by the National Science Foundation through the San Diego Supercomputer Center.

Appendix: Rate Equation Coefficients

The coefficients of linear growth and self- and cross-saturation are

$$\alpha_{n\,\mathrm{reduce}} = \int_0^{\bar{L}} w_n^*(\bar{z}) \left\{ u_n(\bar{z}) - i\, v_n(\bar{z}) \right\} d\bar{z} \quad ,$$

$$\beta_{n\,\mathrm{reduce}} = -i \int_0^{\bar{L}} w_n^*(\bar{z}) \left\{ \int_0^{\bar{z}} \left[2\, u_n^*(\bar{z}') \int_0^{\bar{z}'} \int_0^{\bar{z}''} u_n^2(\bar{z}''') \, d\bar{z}''' \, d\bar{z}'' + u_n^*(\bar{z}')\, v_n^2(\bar{z}') - \int_0^{\bar{z}'} u_n^2(\bar{z}'')\, v_n^*(\bar{z}'')\, d\bar{z}'' \right] d\bar{z}' \right\} d\bar{z}$$

$$\gamma_{nv\,\text{reduce}} = -2i\int_0^{\bar{L}} w_n^*(\bar{z})\left\{\int_0^{\bar{z}}\left[2\,u_v^*(\bar{z}')\int_0^{\bar{z}'}\int_0^{\bar{z}''} u_n(\bar{z}''')\,u_v(\bar{z}''')\,d\bar{z}'''\,d\bar{z}'' + u_v^*(\bar{z}')\,v_n(\bar{z}')\,v_v(\bar{z}') - \int_0^{\bar{z}'} u_n(\bar{z}'')\,u_v(\bar{z}'')\,v_v^*(\bar{z}'')\,d\bar{z}''\right]d\bar{z}'\right\}d\bar{z} \quad , \tag{A1}$$

where $w_n(\bar{z}) = f_Q(\bar{z})\,e^{i\Delta_n\bar{z}}$, $u_n(\bar{z}) = \int_0^{\bar{z}} w_n(\bar{z}')\,d\bar{z}'$, and $v_n(\bar{z}) = \int_0^{\bar{z}} u_n(\bar{z}')\,d\bar{z}'$.

REFERENCES

1 A. H. McCurdy and C. M. Armstrong, Phys. Rev. Lett. **61**, 2316 (1988).

2 W. E. Lamb, Jr., Phys. Rev. A **134**, 1429 (1964).

3 G. S. Nusinovich, Int. J. Electron. **51**, 457 (1981).

4 E. E. David, Jr., Proc. IRE **40**, 669 (1952).

5 J. C. Slater, in *Micronotes* (Microwave Associates, Burlington, MA, 1966), Vol. 4, p. 2.

6 B. Vyse and H. Levinson, IEEE Trans. Microwave Theory Tech. **29**, 739 (1981).

7 A. H. McCurdy and C. M. Armstrong, IEEE Trans. Microwave Theory Tech. **36**, 891 (1988).

8 J. Lachambre, P. Lavigne, G. Otis, and M. Noël, IEEE J. Quantum Electron. **12**, 756 (1976).

9 Y. K. Park, G. Giuliani, and R. L. Byer, IEEE J. Quantum Electron. 20, 117 (1984).

10 K. R. Chu, Phys. Fluids **21**, 2354 (1978).

11 J. C. Slater, *Microwave Electronics* (Van Nostrand, New York, 1950), p. 205.

12 A. H. McCurdy, A. K. Ganguly, and C. M. Armstrong, Phys. Rev. A **40**, 1402 (1989).

13 A. H. McCurdy, C. M. Armstrong, W. M. Bollen, R. K. Parker, and V. L. Granatstein, Phys. Rev. Lett. **57**, 2379 (1986).

14 Rand Publication CP78, *Reduce User's Manual Version 3.2*, edited by A.C. Hearn (The Rand Corp., Santa Monica, CA, 1985).

15 S.O. Rice, Bell Syst. Tech. J. **24**, 100 (1945).

16 F. E. Ehlers, in *Microwave Transmission Circuits* , edited by G. L. Ragan (McGraw-Hill, New York, 1948), p. 369.

17 A. W. Fliflet, M. E. Read, K. R. Chu, and R. Seeley, Int. J. Electron. **53**, 505 (1982).

TABLE I

Calculated rate equation coefficients corresponding to the experiment: beam voltage 19.98 kV, beam current .34 A, $\alpha = 1.4$, magnetic field of 1.838 kG.

TE_{111}	TE_{112}	TE_{113}	TE_{114}
$\alpha_1 = .321$	$\alpha_2 = .476$	$\alpha_3 = .349$	$\alpha_4 = .31$
$\beta_1 = -.0048$	$\beta_2 = .0092$	$\beta_3 = .017$	$\beta_4 = .018$
$\gamma_{12} = -.0088$	$\gamma_{21} = .0079$	$\gamma_{31} = .0195$	$\gamma_{41} = .027$
$\gamma_{13} = -.0075$	$\gamma_{23} = .0213$	$\gamma_{32} = .0324$	$\gamma_{42} = .0388$
$\gamma_{14} = -.0008$	$\gamma_{24} = .0208$	$\gamma_{34} = .037$	$\gamma_{43} = .042$

FIGURE CAPTIONS

1: Configuration of the ECM with inset showing the midplane probe geometry.

2: (a) Magnetic field dependence of the $Im\{\alpha_n\}$ for various modes. Positive $Im\{\alpha_n\}$ means linear growth. (b) Linear predictions of the oscillation frequency [from $Re\{\alpha_n\}$] as a function of magnetic field.

3: Mode evolution for two strongly coupled modes. Arrows indicate the direction of increasing time.

4: Mode priming of the ECM. (a) Free oscillation skipping between the TE_{111} (upper trace) and the TE_{113} modes. (b) Pure TE_{111} mode primed operation (injected signal frequency equals TE_{111} frequency of 5.093 GHz). (c) Pure TE_{113} mode primed operation (injected signal frequency is 5.141 GHz). (d) Relative phase between the TE_{111} oscillation and priming signal corresponding to the experiment shown in (b).

5: Temporal dependence of mode priming. The top trace in each shows detector measurement of rf drive power while the bottom measures ECM output power. (a) No drive signal, mode skipping between TE_{111} (lower) and TE_{113} (upper). (b) Drive signal applied too early in buildup. (c) Optimal application time of drive pulse. (d) Drive pulse applied too late.

6: Enlargement of the region of pure TE_{111} mode oscillation due to a 20-W drive signal at the oscillation frequency (shaded). Regions of displaced pure mode operation are indicated.

7: Minimum drive power required to prime a pure TE_{111} mode from pure TE_{112} as a function of frequency separation between the drive signal and TE_{111} oscillation.

8: Geometry for (a) one-probe and (b) two-probe excitation.

9: Mode control as a function of normalized power into the left-hand circularly polarized electromagnetic wave. The three experiments involve driving one probe, two probes with equal power and 90^{o} phase lead on probe #1, and two probes at 90^{o} with unequal power.

10: Degree of mode control as a function of phase shift between probes. Phase shifts corresponding to pure right-hand (dot) and left-hand (dash) waves are indicated.

11: Effective power on the electron orbit as a function of relative phase between probes. The line shows theory for a left- to right-hand coupling ratio of 55.2.

12: Universal curves of TE_{111} coefficients for different detuning parameters : (a) α_1 , (b) β_1 , (c) γ_{12} with real part (dash) and imaginary part (solid).

13: Universal curves of TE_{112} coefficients for different detuning parameters: (a) α_2 , (b) β_2, (c) γ_{21} with real part (dash) and imaginary part (solid).

14: Imaginary part of the coefficients for the three lowest order axial modes vs. magnetic field: (a) TE_{111} , (b) TE_{112} , (c) TE_{113}. The respective scale and dimensions are α , (ns^{-1}); $\beta \times 2 \times 10^{-8}$, (J^{-1}) ; $\gamma \times 2 \times 10^{-8}$, (J^{-1}) .

15: Mode evolution for the experimental case including fifth order coupling terms.

16: Degree of mode control achieved with a given drive power and .3 μW noise power. Error bars show the standard deviation in predicted control.

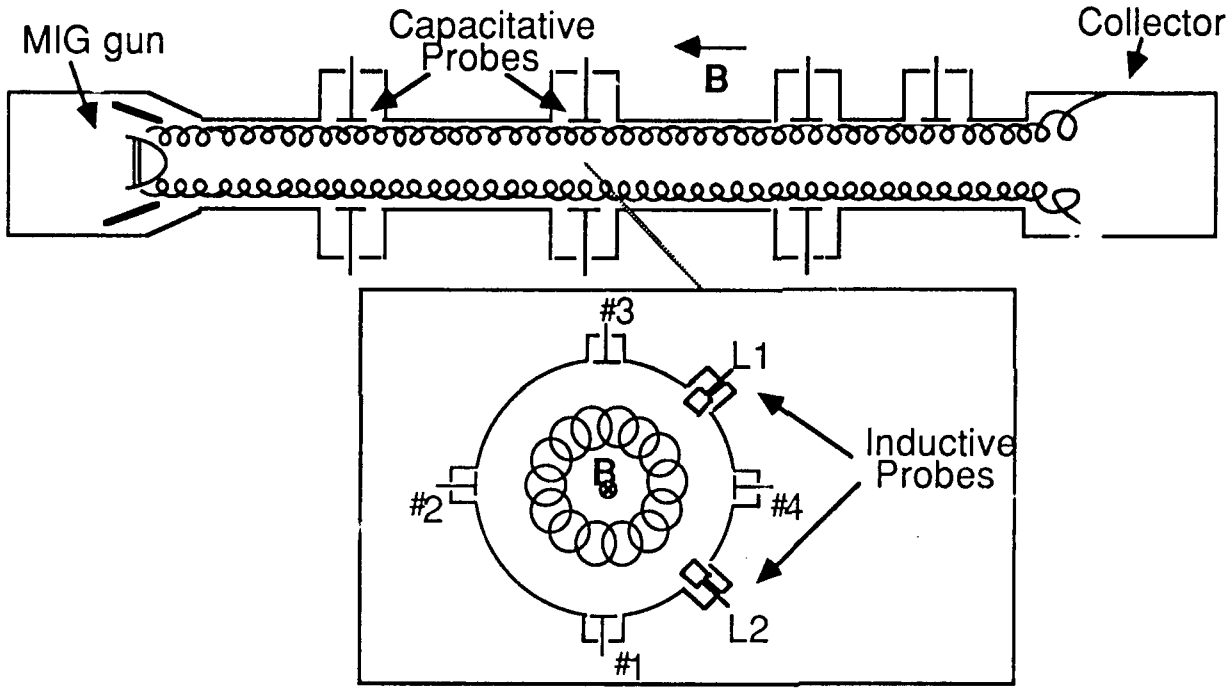
MIG gun
Capacitative Probes
B
Collector
#3
L1
Inductive Probes
#2
B
#4
L2
#1

FIG. 1

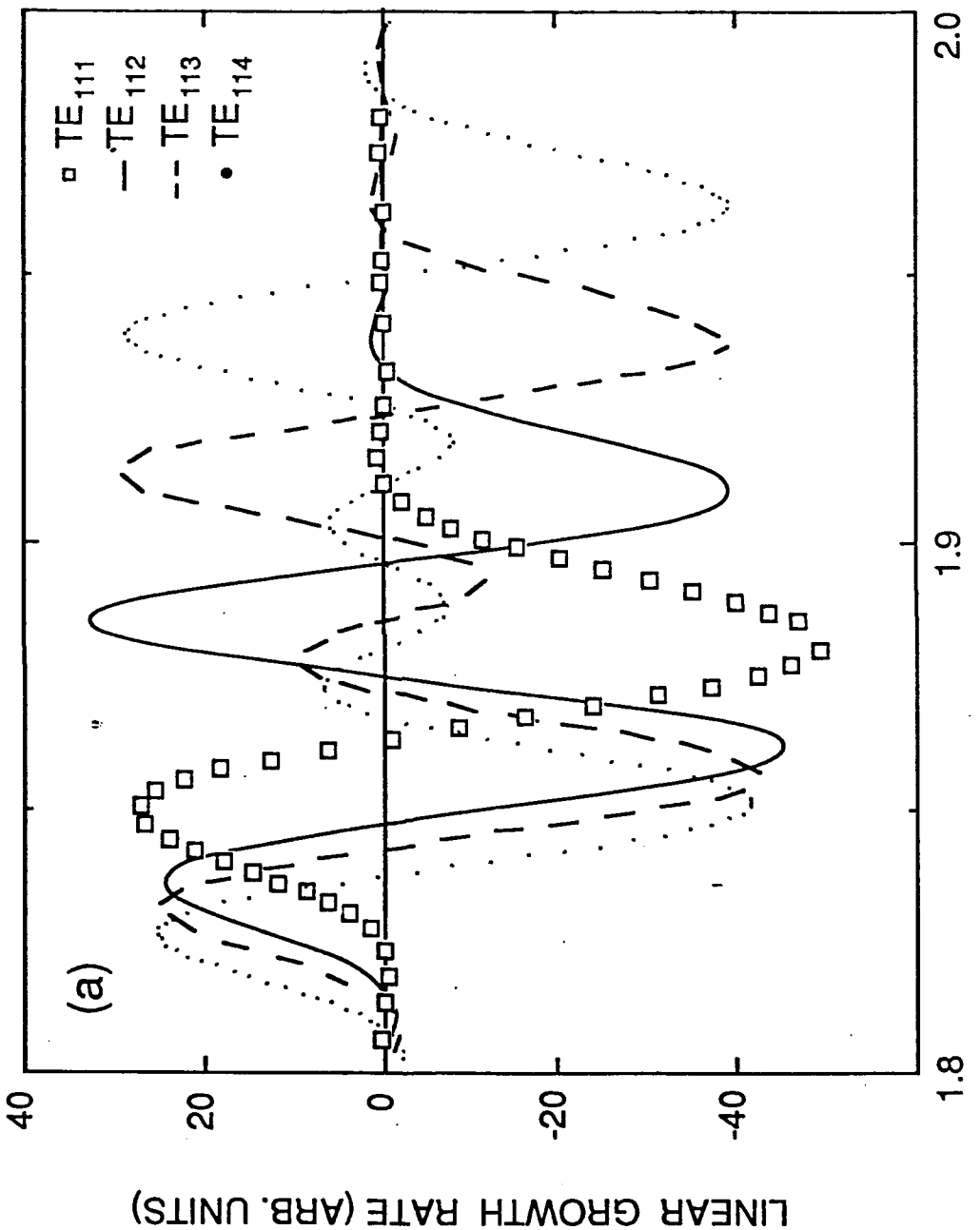
TE111
TE112
TE113
TE114
(a)
40
20
0
-20
-40
1.8
1.9
2.0
LINEAR GROWTH RATE (ARB. UNITS)
MAGNETIC FIELD (KG)

FIG. 2(a)

FIG. 2 (b)

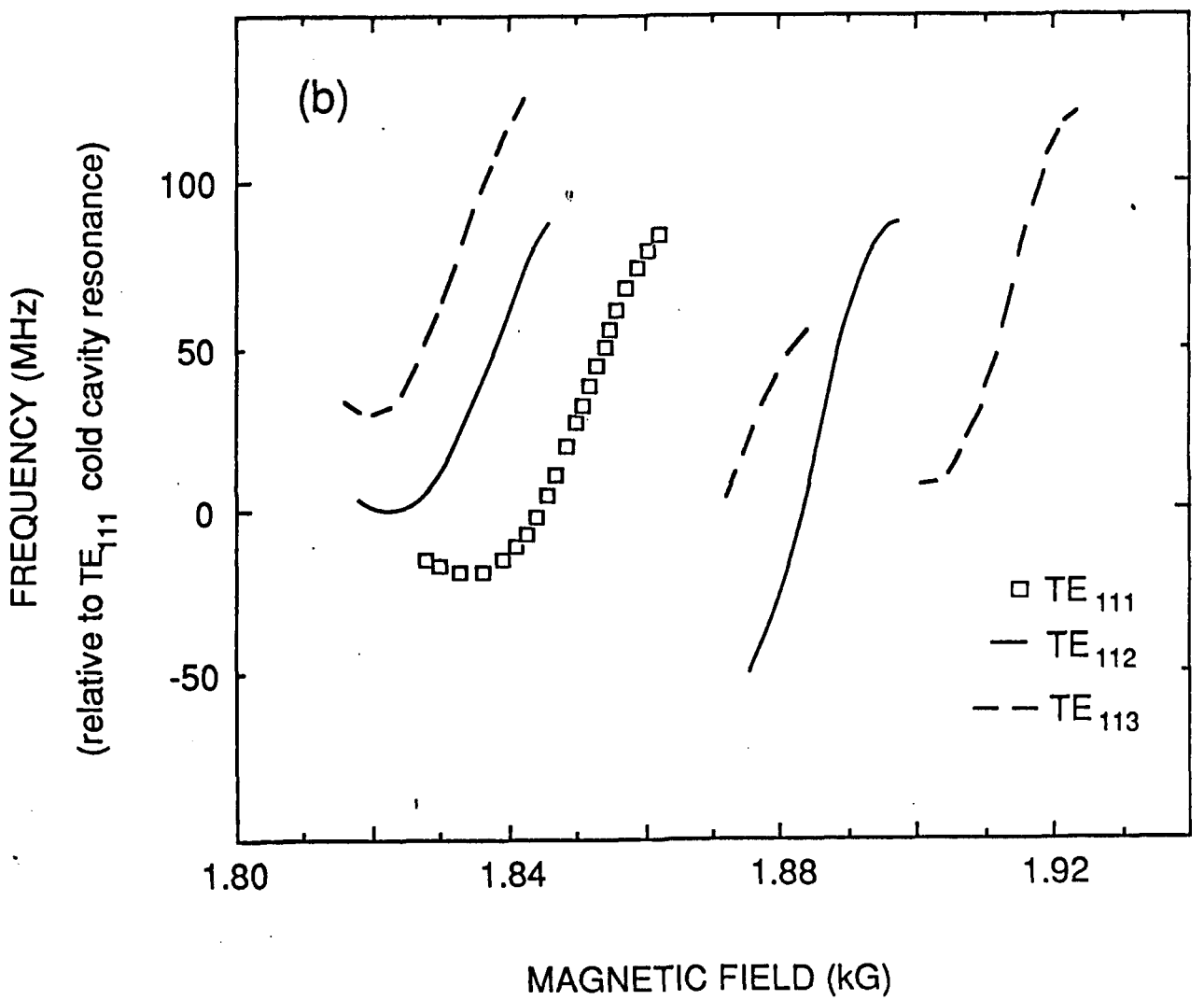
(b)
100
50
0
-50
1.80
1.84
1.88
1.92
FREQUENCY (MHz)
(relative to TE111 cold cavity resonance)
MAGNETIC FIELD (kG)
TE111
TE112
TE113

FIG. 3

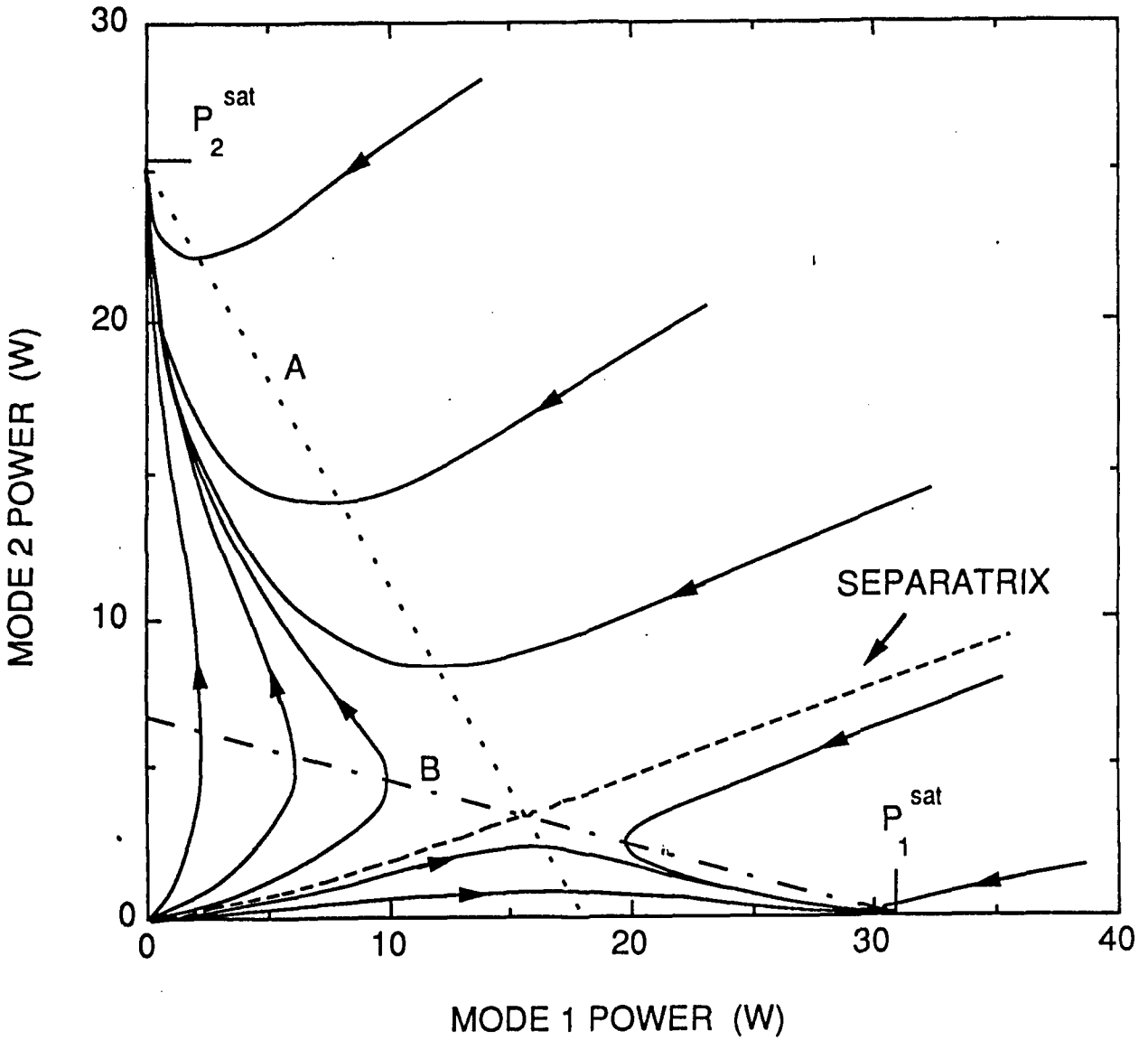
30
20
10
0
0
10
20
30
40
MODE 2 POWER (W)
MODE 1 POWER (W)
P2 sat
A
B
SEPARATRIX
P1 sat

(a)

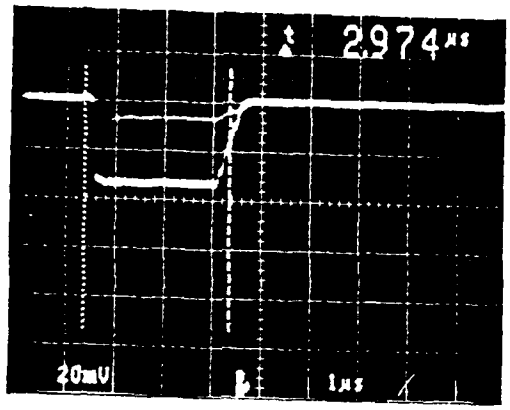

(b)

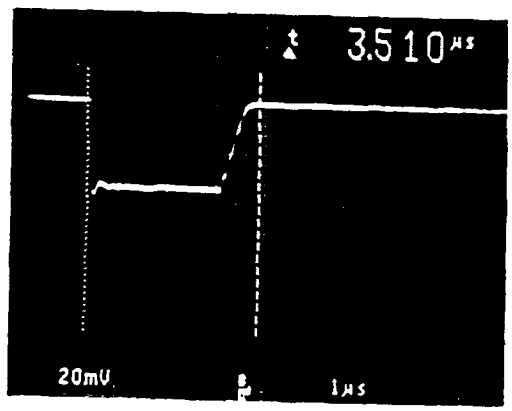

(c)

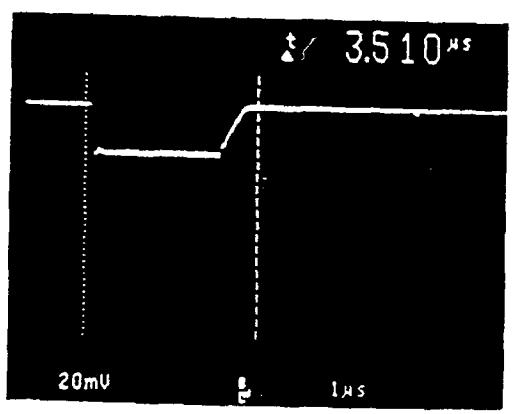

(d)

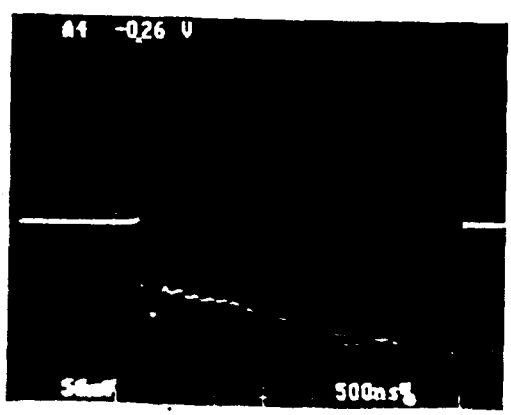

FIG. 4

(a)

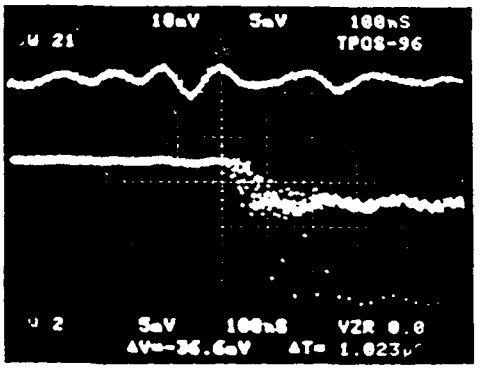
10mV 5mV 100nS
TPOS-96
5mV 100nS VZR 0.0

(b)

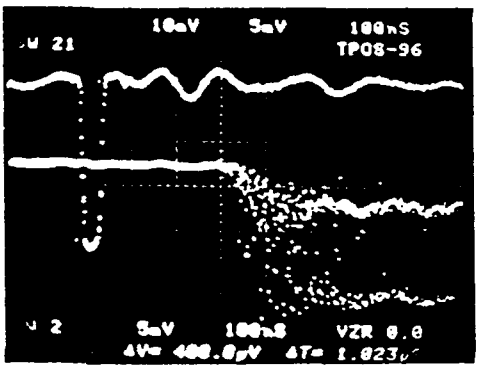
10mV 5mV 100nS
TPOS-96
5mV 100nS VZR 0.0

(c)

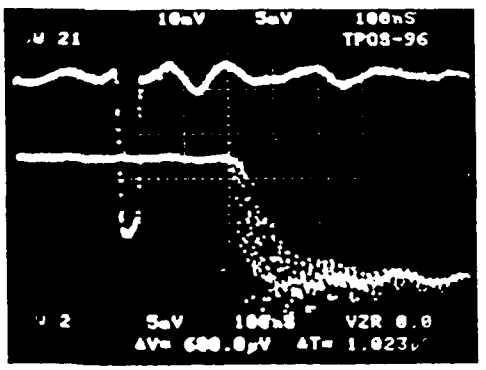
10mV 5mV 100nS
TPOS-96
5mV 100nS VZR 0.0

(d)

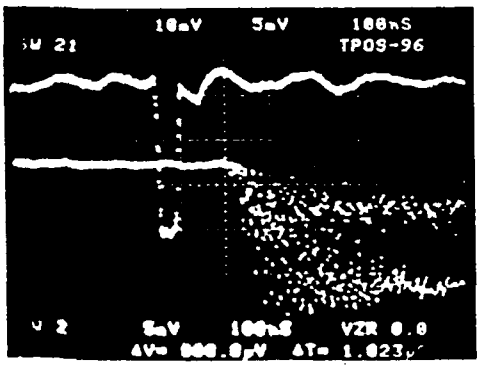
10mV 5mV 100nS
TPOS-96
5mV 100nS VZR 0.0

FIG. 5

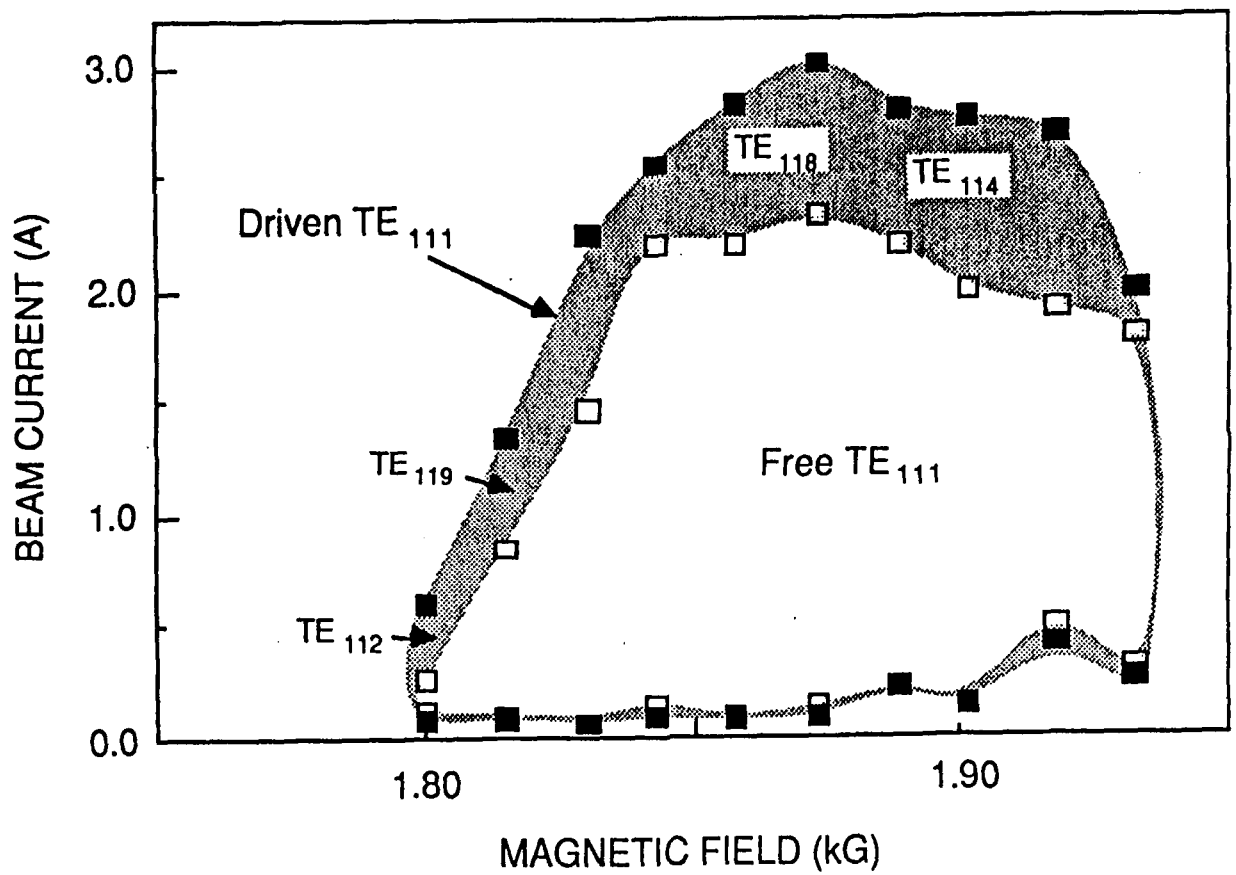
3.0
2.0
1.0
0.0
BEAM CURRENT (A)
Driven TE 111
TE 118
TE 114
TE 119
Free TE 111
TE 112
1.80
1.90
MAGNETIC FIELD (kG)

FIG. 6

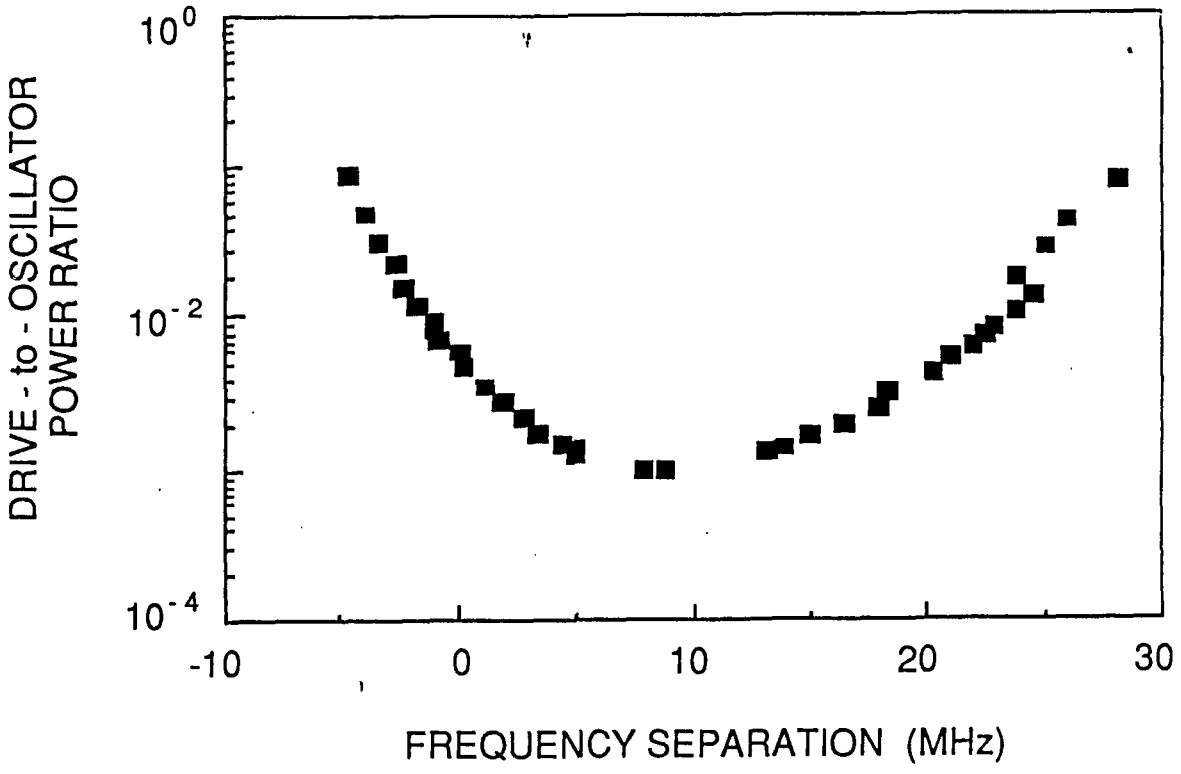
DRIVE - to - OSCILLATOR POWER RATIO
10^0
10^{-2}
10^{-4}
-10
0
10
20
30
FREQUENCY SEPARATION (MHz)

FIG. 7

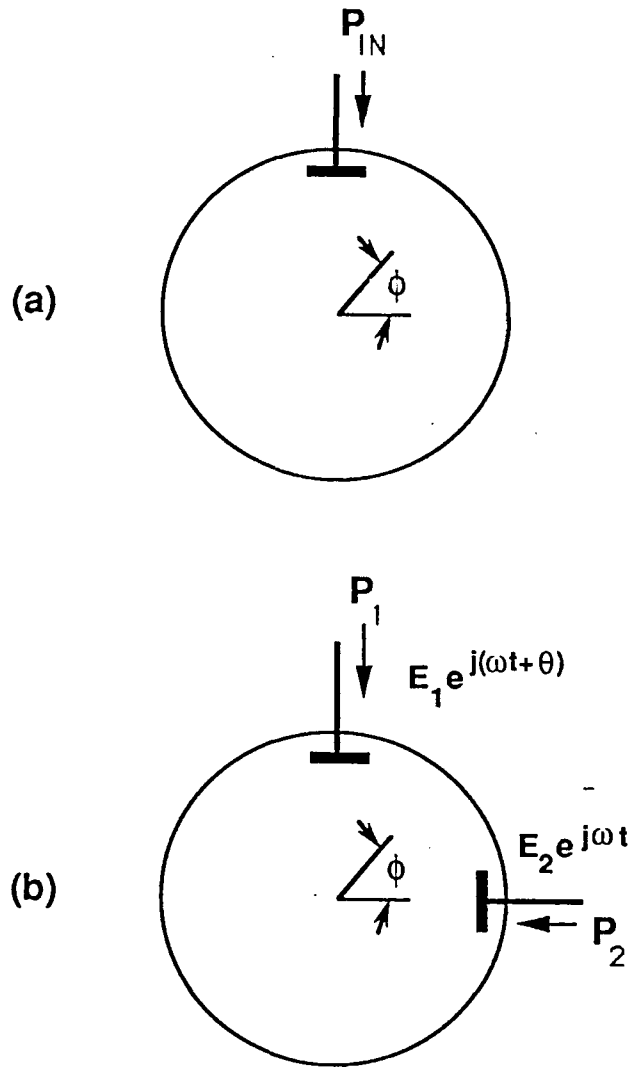

FIG. 8

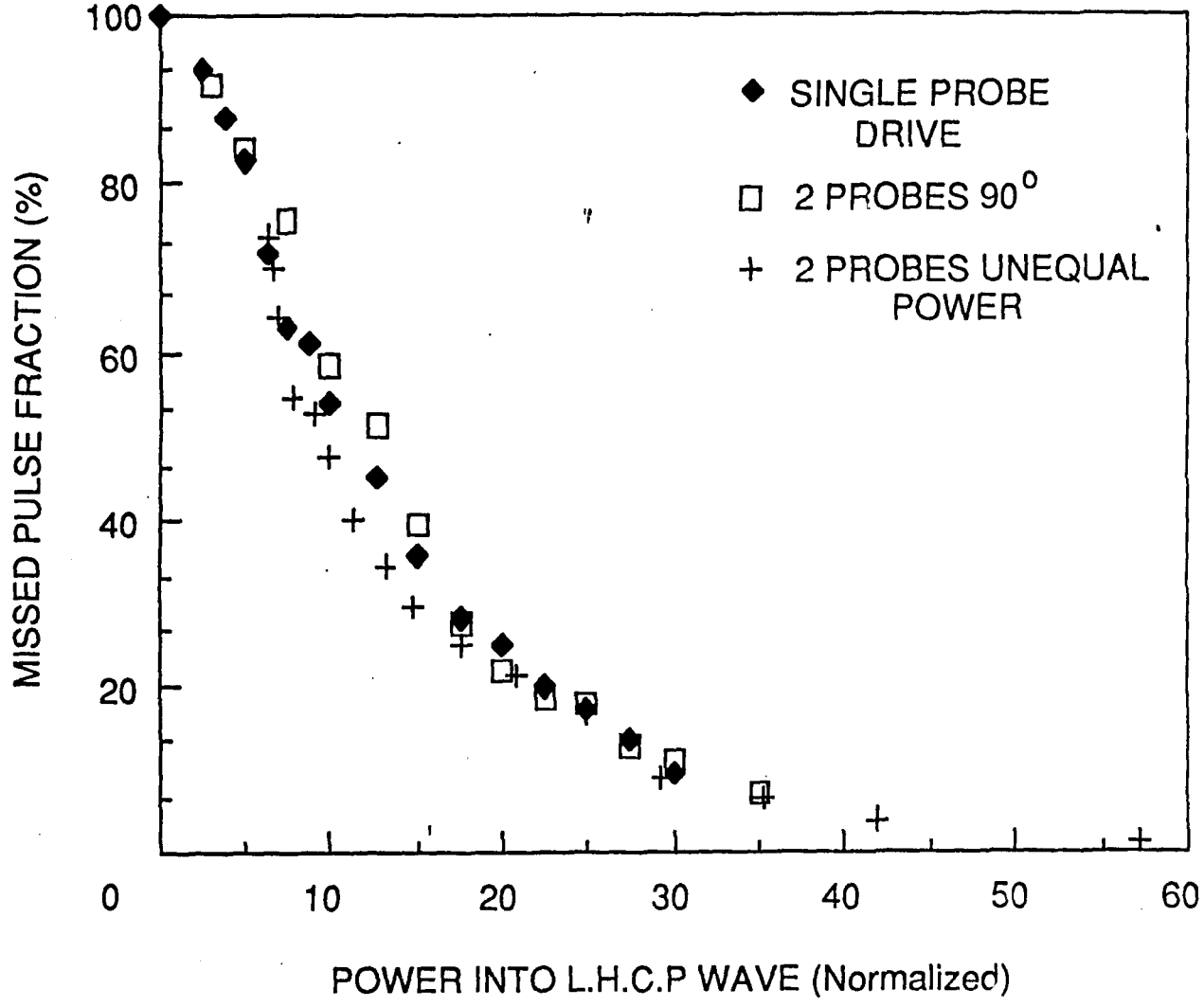
100
80
60
40
20
0
10
20
30
40
50
60
MISSED PULSE FRACTION (%)
POWER INTO L.H.C.P WAVE (Normalized)
SINGLE PROBE DRIVE
2 PROBES 90°
2 PROBES UNEQUAL POWER

FIG. 9

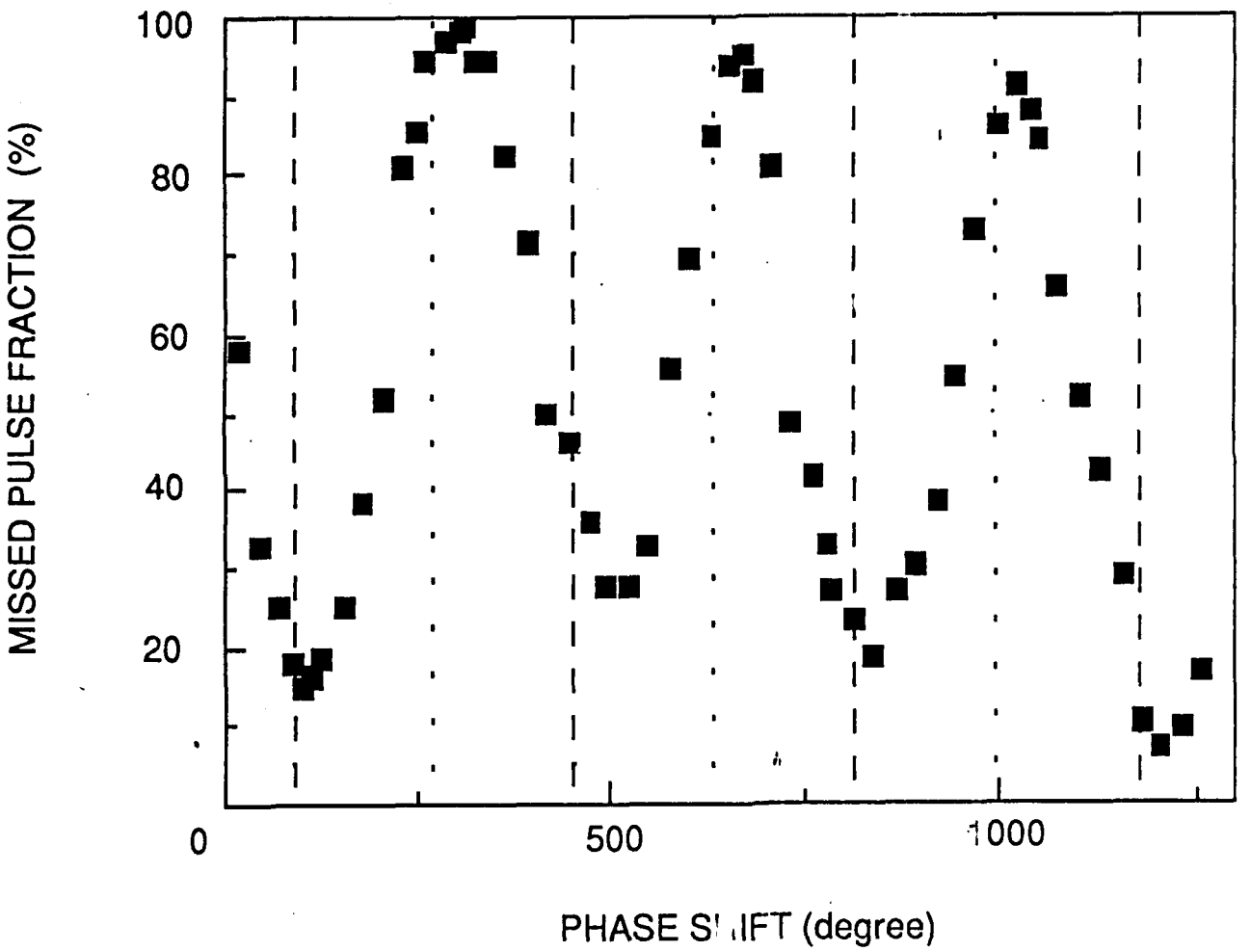
MISSED PULSE FRACTION (%)
100
80
60
40
20
0
500
1000
PHASE SHIFT (degree)

FIG. 16

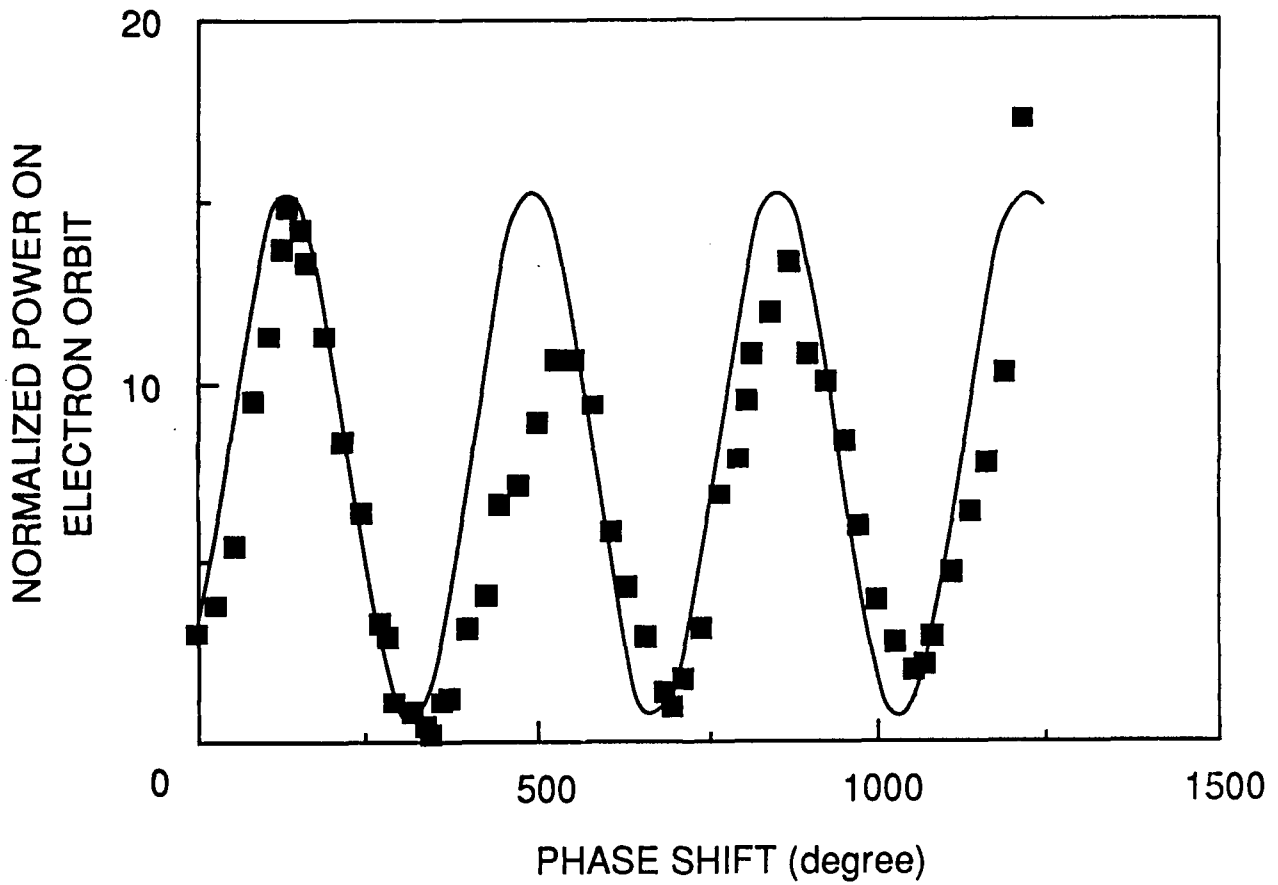
20
10
0
500
1000
1500
NORMALIZED POWER ON ELECTRON ORBIT
PHASE SHIFT (degree)

FIG. 11

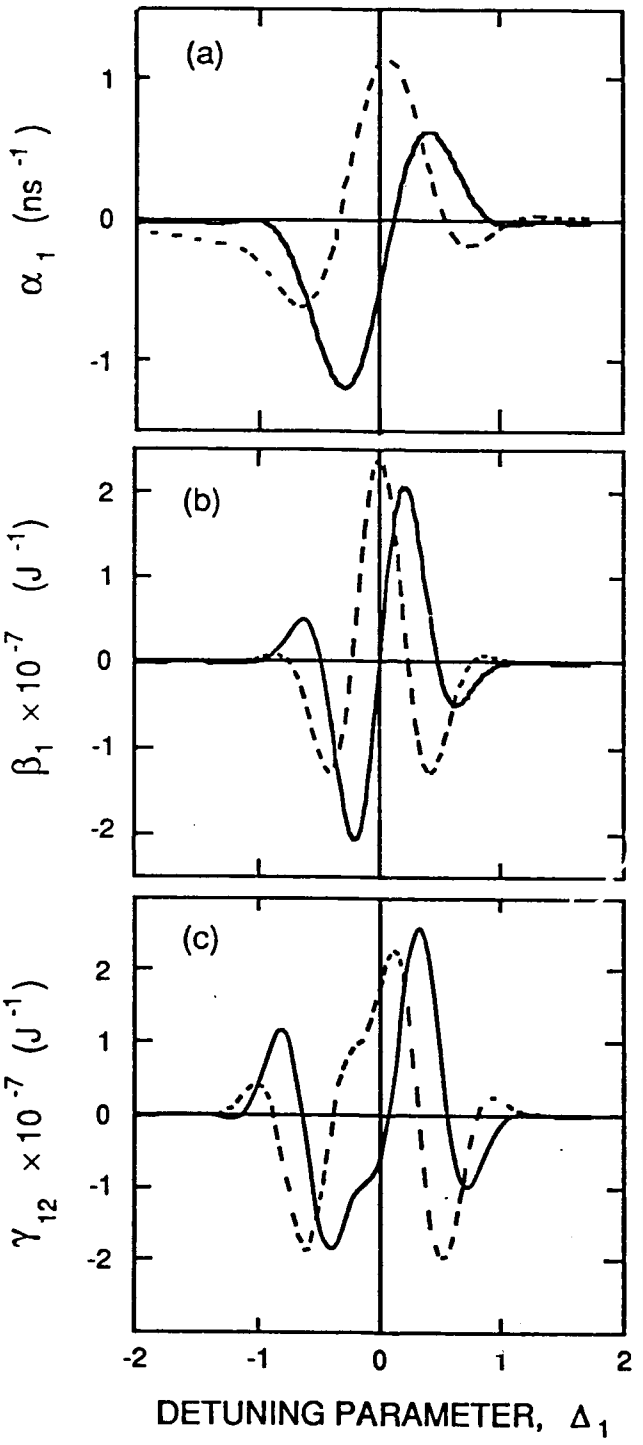
(a)
(b)
(c)
α_1 (ns^{-1})
$\beta_1 \times 10^{-7}$ (J^{-1})
$\gamma_{12} \times 10^{-7}$ (J^{-1})
1
0
-1
2
-2
-2
-1
0
1
2
DETUNING PARAMETER, Δ_1

FIG. 12

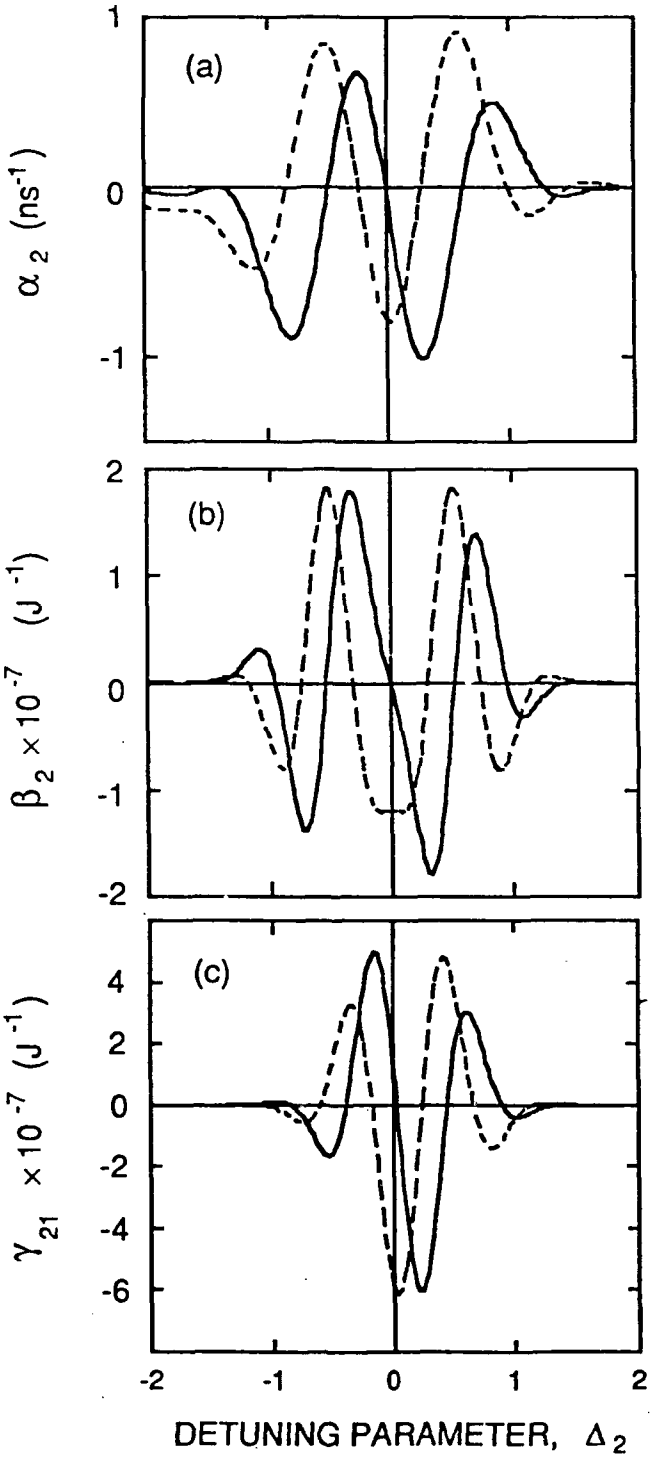
(a)
(b)
(c)
α_2 (ns^{-1})
$\beta_2 \times 10^{-7}$ (J^{-1})
$\gamma_{21} \times 10^{-7}$ (J^{-1})
DETUNING PARAMETER, Δ_2

FIG. 13

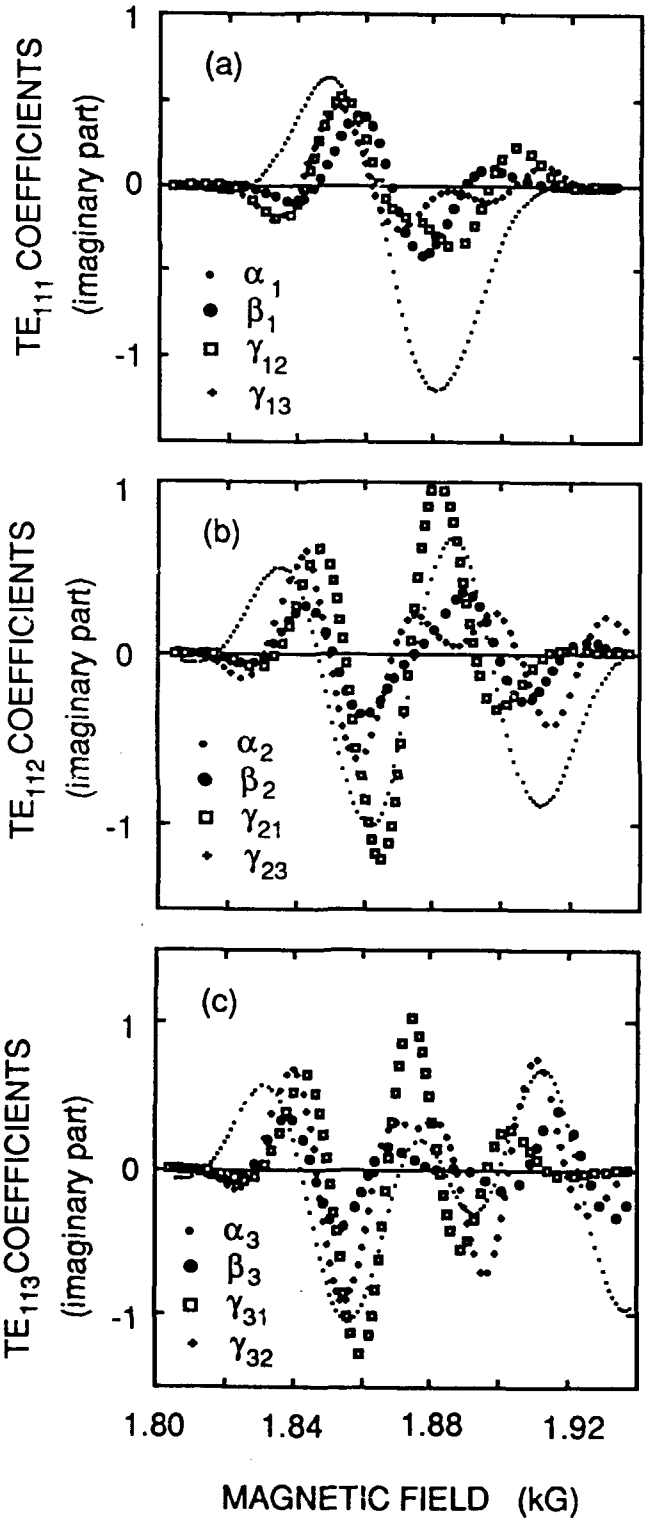
(a)
(b)
(c)
TE111 COEFFICIENTS
(imaginary part)
TE112 COEFFICIENTS
(imaginary part)
TE113 COEFFICIENTS
(imaginary part)
α1
β1
γ12
γ13
α2
β2
γ21
γ23
α3
β3
γ31
γ32
1
0
-1
1.80
1.84
1.88
1.92
MAGNETIC FIELD (kG)

FIG. 14

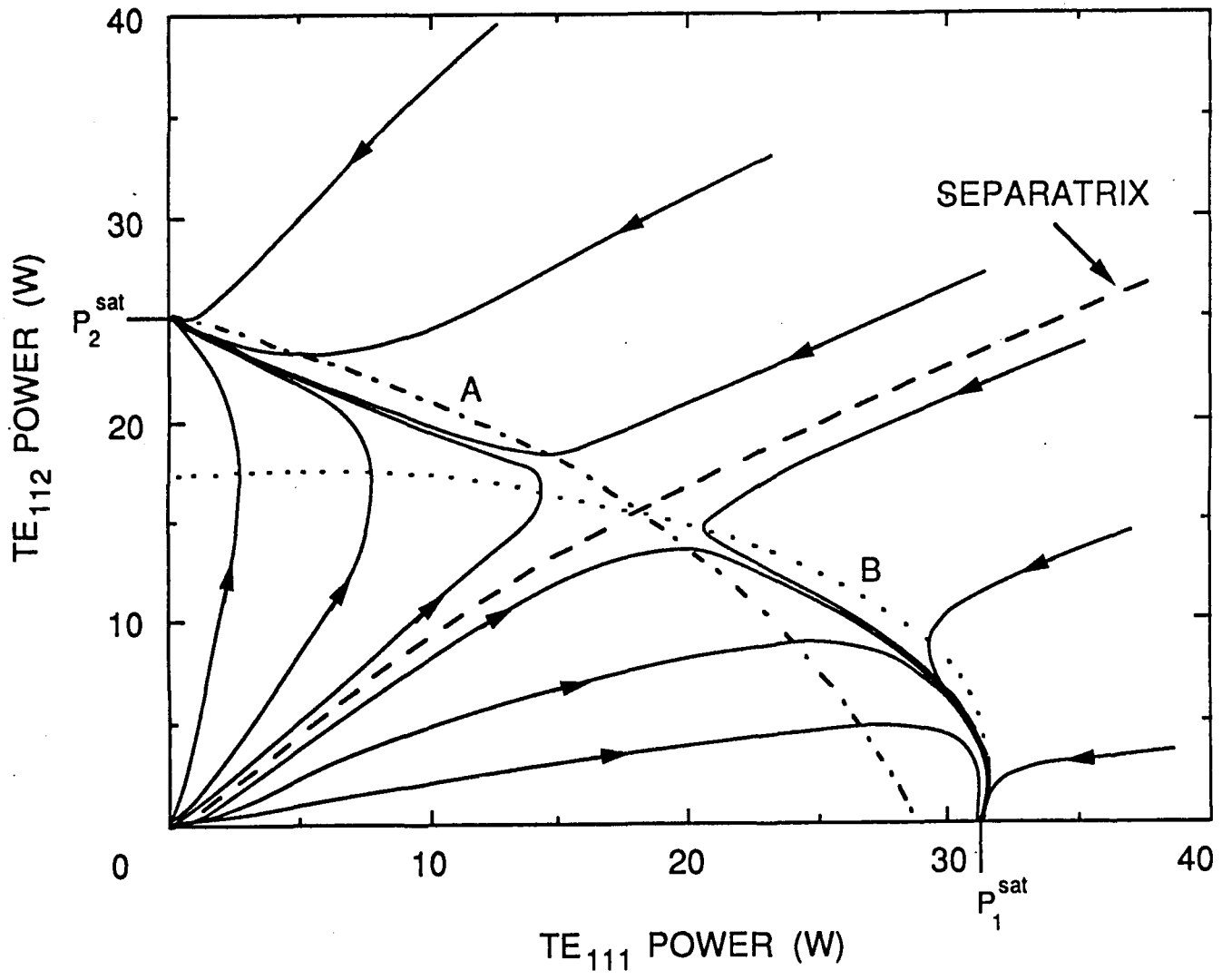
40
30
20
10
0
10
20
30
40
P_2^{sat}
P_1^{sat}
SEPARATRIX
A
B
TE_{112} POWER (W)
TE_{111} POWER (W)

FIG. 15

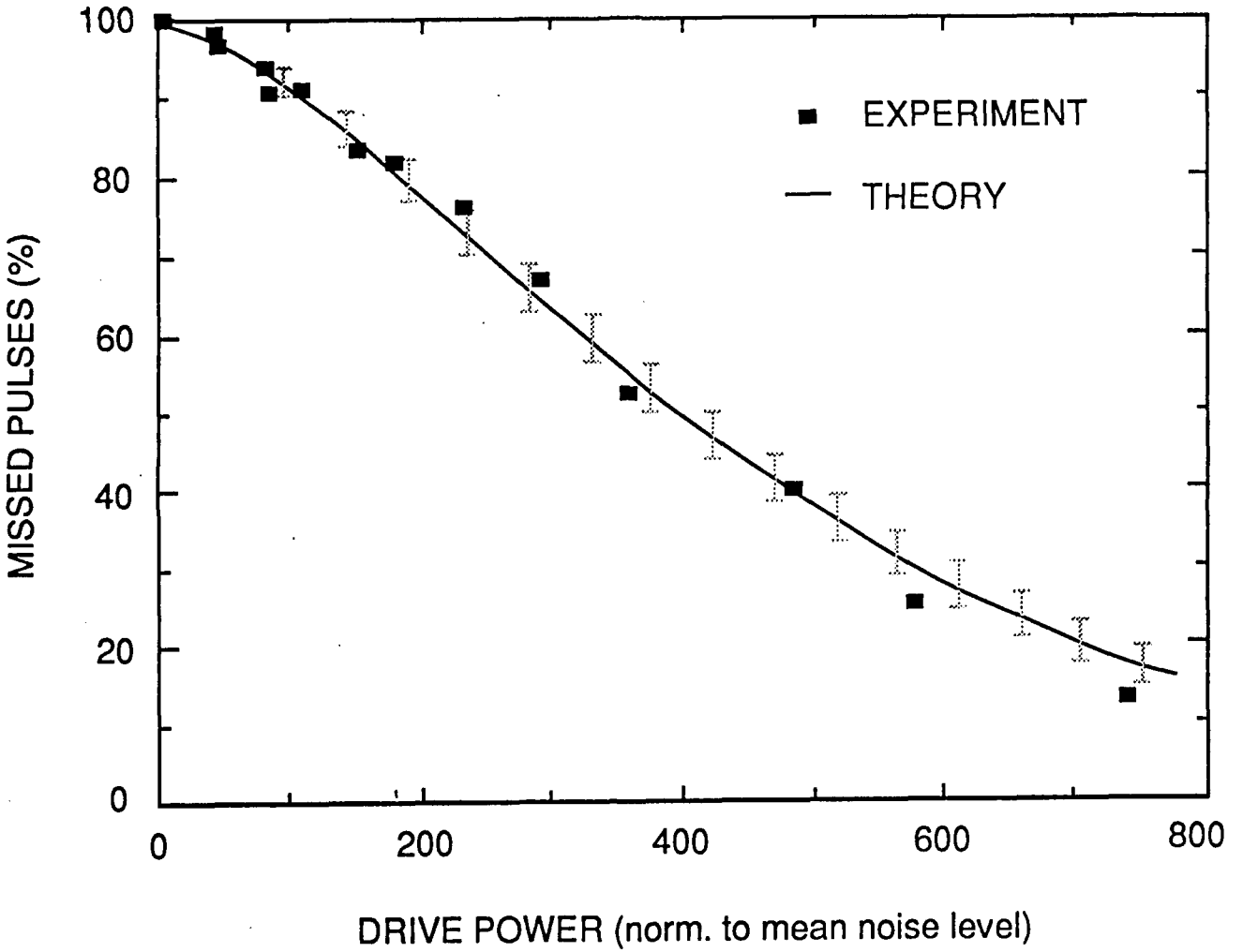
100
80
60
40
20
0
MISSED PULSES (%)
EXPERIMENT
THEORY
0
200
400
600
800
DRIVE POWER (norm. to mean noise level)

FIG. 16